Dynamic response analysis of a catamaran installation vessel during the positioning of a wind turbine assembly onto a spar foundation

Zhiyu Jiang[a,b], Lin Li[c,*], Zhen Gao[a,b,d], Karl Henning Halse[b,e], Peter Christian Sandvik[b,f]

[a]*Department of Marine Technology, Norwegian University of Science and Technology (NTNU)*
[b]*Centre for Research-based Innovation of Marine Operations (SFI MOVE), NTNU*
[c]*Department of Mechanical and Structural Engineering and Materials Science, University of Stavanger*
[d]*Centre for Autonomous Marine Operations and Systems (SFF AMOS), NTNU*
[e]*Department of Ocean Operations and Civil Engineering, NTNU*
[f]*PC Sandvik Marine, Trondheim, Norway*

Abstract

Installation of floating wind turbines is a challenging task. The time and costs are closely related to the installation method chosen. This paper investigates the performance of an efficient installation concept – a catamaran wind turbine installation vessel. The vessel carries pre-assembled wind turbine units including towers and rotor nacelle assemblies. Each unit is placed onto a pre-installed offshore support structure (in this paper a spar floater) during installation. The challenge is to analyse the responses of the multibody system (catamaran-spar-wind turbine) under simultaneous wind and wave loads. Time-domain simulations were conducted for the coupled catamaran-spar system with mechanical coupling, passive mooring system for the spar, and dynamic positioning control for the catamaran. We focus on the steady-state stage prior to the mating process between one turbine unit and the spar, and discuss the effects of wind loads and wave conditions on motion responses of the catamaran and the spar, relative motions at the mating point, gripper forces and mooring forces. The relative motion at the mating point is less sensitive to the blade orientation, but influenced by the wave conditions. Under the investigated sea states, the present installation method shows decent performance.

Keywords: catamaran; floating wind turbine; offshore installation; dynamic response; outcrossing; wind and waves

*Corresponding author
Email addresses: zhiyu.jiang@ntnu.no (Zhiyu Jiang), lin.li@uis.no (Lin Li), zhen.gao@ntnu.no (Zhen Gao), karl.h.halse@ntnu.no (Karl Henning Halse), pcsandvik@gmail.com (Peter Christian Sandvik)

1. Introduction

Renewable energy resources have attracted broad interests worldwide, because of the increasing demand for energy and concerns about global warming. Among the various sources of renewable energy, wind energy is among the most rapidly developing one, with energy production at an annual growth rate of 25–30% [1]. At the end of 2016, Europe's cumulative installed offshore wind capacity reached 12631 megawatt (MW). 81 offshore wind farms across 10 European countries had been constructed, with an average capacity rating of 4.8 MW per turbine and an average water depth of 29.2 meters (m) [2].

Because of the high-quality wind resources and geographical limitations, several countries are considering deep water offshore areas for future development of wind power facilities. In deep water of more than 150 m, floating foundations are more cost effective than bottom-fixed ones. Different forms of floating foundations have been proposed. Spar, tension leg platform, and semi-submersible types are most promising. Although the technologies are proven and have been applied to the oil and gas industry, commercial deployment is still at an early stage because of costs. The Hywind pilot park, the world's first floating wind farm, is expected to produce power in late 2017 [3].

Research of offshore wind technologies has been gaining momentum since 2000s. With the development and maturity of the state-of-the-art numerical simulation tools [4, 5, 6], coupled dynamic analysis of offshore wind turbines (OWTs) becomes possible. Still, most of the related literature is focused on design and analysis of OWTs in various operational or parked conditions [7, 8, 9, 10, 11]. In contrast, there is limited research work on installation of OWTs. Sarkar et al. [12] presented the technical feasiblity of an installation concept using a floating vessel along with a floatable subsea structure for installing monopile-type OWTs. Guachamin-Acero et al. [13] developed an installation concept for small crane vessels using the inverted pendulum principle in which the pre-assembled rotor, nacelle and tower can be installed via rotation through a rotating frame at the tower base. Ahn et al. [14] evaluated various methods of wind turbine installation in the Korean west-south wind farm and analysed the instalaltion cost of OWTs. Paterso et al. [15] considered the installation modelling for UK offshore wind Rounds 1 and 2 using a probabilistic simulation tool and provided a quantification of installation vessel performance to support developers and project planners. Esteban et al. [16] reviewed the processes and methods employed in the offshore installation of the most relevant types of gravity-based structures in offshore wind facilities operating in Europe.

To reduce the cost of offshore installations, one primary challenge is to increase the weather window and to avoid unexpected delays. To achieve this, accurate assessment is desired of the performance of the installation vessels and installation methods, and numerical methods and models have been developed to estimate systems' dynamic responses during installation. Most of the studies focused on static [17] or steady-state dynamic responses [18], whereas in a few studies, the nonstationary features of the installation process were also considered [19, 20]. Based on numerical simulations and response-based criteria, methodologies for assessment of allowable sea states for installing OWTs can be established. So far, these methodologies have been applied to monopile foundation installation [21] and transition piece installation [22] of bottom-fixed OWTs.

Compared to bottom-fixed OWTs with monopile, gravity-based, or jacket foundations [23], floating wind turbines are born with even more challenges with regard to transportation, assembly, and installation. Consider the installation of Hywind, which is a spar-type floating wind turbine. In order to increase the operability, the upending and assembly was done at a well-sheltered location. Then the unit was towed to the site and hooked up to the mooring system [24]. For OWT installations, the tower, nacelle, and blades can be either pre-assembled and installed by a single lift [25], or separated and installed piece by piece in a split way [26, 27]. In the Hywind installation challenge campaign [28], and among the proposed innovative installation concepts, there is a tendency to favour novel installation vessels and facilities to reduce offshore lifts and operation time. A novel wind turbine installation concept has been recently proposed by the SFI MOVE project [29, 30]. Fig. 1 gives an overview of the concept, which uses a catamaran installation vessel for installations of OWTs, and can be used for offshore bottom-fixed or floating foundations. The aim of this concept is to avoid extremely weather-sensitive high lifts from a floating vessel.

The concept is in its infancy, and to demonstrate the feasibility of the concept, numerical simulations and model tests should be performed. Compared to single floating bodies, behaviour of the coupled catamaran-spar system will be more complex, because of mechanical and hydrodynamic couplings between the floating bodies. It is necessary to identify the motion characteristics of the system, under various environmental conditions. For a proper design of the mechanical grippers, the coupling forces acting on them should be accurately estimated. Additionally, the relative motions between the pre-assembled wind turbine and the spar foundation should be limited in order to connect them.

This study presents the numerical modelling and results of the catamaran-spar system with a

focus on the dynamic behaviour of the concept during the stage when a wind turbine assembly is being positioned above the spar top. First, the installation concept is briefly introduced in Section 2. Section 3 shows modelling details of the system. Based on time-domain simulations of the coupled system under wind-wave conditions, we present in Section 4 the motion characteristics of the system, critical parameters to the mating, forces on the sliding grippers, and mooring line forces of the spar. Finally, conclusions are drawn in Section 5.

2. The catamaran installation vessel concept

2.1. General

The catamaran installation vessel is designed to carry a maximum of four pre-assembled wind turbines on board. Compared to existing installation methods that require multiple lifts of wind turbine components offshore, this concept minimises the number of offshore lifts and installations, and therefore the operational time. The reduced operational time implies a potential for cost reduction. However, as gigantic MW-sized turbine assemblies are handled offshore, a specialised vessel with complex mechanisms must be properly designed. Fig. 2 presents the main components: a catamaran, a floating spar foundation, sliding grippers in the aft of the catamaran, and lifting grippers on the deck. During installations, the sliding grippers connect the floating spar to the catamaran and constrain their motions in the horizontal plane. The lifting grippers should be able to hold a turbine assembly of more than 1000 Tonnes. Standard industrial heave compensation systems with acceleration feedback or feedforward [31, 32] can be applied to the lifting grippers to minimise the impact forces that occur during the mating phase. The spar foundation has a passive mooring system, whereas the catamaran is thruster assisted using a dynamic positioning (DP) system. During installation, when the catamaran and the spar foundation are connected, the waves will propagate parallel to the catamaran's heading in ideal situations.

Table 1 summarises properties of the catamaran and the spar. The hydrostatic stability of the catamaran was checked for various loading conditions [30], and the fully loaded condition was considered in this work. Mass properties of the spar foundation were scaled from in-house data.

2.2. Installation procedure

Fig. 3 shows the proposed main steps for the complete installation of a wind turbine assembly on a floating foundation, and selected steps are illustrated in Fig. 4. The installation process

Table 1: Selected properties of the studied catamaran-spar system

Parameter	*Symbol*	*Value*
Catamaran with four wind turbines		
Length overall (m)	L_{OA}	144
Breath moulded (m)	B	60
Spacing between mono-hulls at waterline (m)	L_{hull}	38
Draft (m)	T_c	8.0
Displacement mass (tonnes)	Δ_c	18502.9
Vertical centre of gravity (COG) above baseline (m)	KG_c	28.6
Transverse metacentric height (m)	GM_t	66.4
Body origin in global coordinate system	(X_c,Y_c,Z_c)	(64,0,0)
Body origin in global coordinate system	(X_s,Y_s,Z_s)	(0,0,0)
Spar foundation alone (before mating)		
Diameter at top (m)	L_{bd1}	9.5
Diameter at waterline (m)	M_{bd1}	14
Draft (m)	T_{s1}	70
Vertical position of centre of buoyancy (m)	Zs_{COB1}	-35
Vertical position of COG (m)	Zs_{COG1}	-51.8
Displacement mass (tonnes)	Δ_{s1}	11045
Vertical position of fairlead (m)	Z_{f1}	-15
Spar foundation with wind turbine assembly (after mating)		
Diameter at top (m)	L_{bd2}	9.5
Diameter at waterline (m)	M_{bd2}	9.5
Draft (m)	T_{s2}	80
Vertical position of centre of buoyancy (m)	Zs_{COB2}	-41.5
Vertical position of COG (m)	Zs_{COG2}	-50
Displacement mass (tonnes)	Δ_{s2}	12160
Vertical position of fairlead (m)	Z_{f2}	-25
Wind Turbine		
Rated power (MW)	RP	10
Rotor mass (tonnes)	M_{rotor}	200
Nacelle mass (tonnes)	$M_{nacelle}$	400
Tower mass (tonnes)	M_{tower}	600

initiates when the catamaran is connected to the floating foundation by sliding grippers. The forecasted weather and the motion measurements are checked in step 2. If the conditions are suitable, the lifting grippers are in action and grasp the tower of the turbine assembly in step 3. The wind turbine assembly is lifted up into the air by the lifting grippers in step 4. In step 5, the assembly is transferred to catamaran's aft by a rack-and-pinion system (not shown). In step 6, relative motions between the floating foundation and the tower bottom are measured by onboard monitoring systems such as Motion Reference Units (MRUs) [33] or OCTOPUS system [34]. These systems provide realtime motion measurements with high accuracy [35]. For a certain time interval, if the relative motion is within allowable limits, the mating between the tower and the foundation takes place (step 7). A cursor system is suggested to increase the tolerance of the mating process, see Fig. 5. The cursor system may consist of a yoke and four guiding beams. A detailed design is beyond the scope of this paper. The mating process is deemed successful after the guiding pins on the tower bottom enter the docking devices inside the floating foundation. Each turbine assembly weighs around 1200 tonnes. When the wind turbine weight has been shifted to the spar, it will increase the draft by approximately 10 m. Because of this change in draft, a provisional mooring system may be needed during the mating phase. To avoid this change, an active ballast system may be employed for the spar. After a successful mating, bolting of the tower structure follows in step 8. Finally, the catamaran releases the floating platform after a successful installation.

2.3. Positioning of a wind turbine assembly

As indicated by Fig. 2, the mating point is located approximately 20 m above the mean water level. At this point, there exist relative motions between the tower bottom and spar top. Large horizontal motions may lead to unsuccessful mating, whereas large vertical motions may cause impact forces during mating. The relative motions in the horizontal plane is emphasised in this study.

The leftmost and middle sketches in Fig. 6 show two possible scenarios in the xy-plane. The tower-bottom motions are closely correlated to the vessel motions, and the spar-top motions are affected by wave loads, mooring system, and mechanical couplings. When the tower and the spar are perfectly aligned along the z-axis, the mating process will be smooth. More often, the two bodies are not always perfectly aligned. η, the relative motion radius, is defined as the distance between the two centres. As η changes over time, it is a function of the relative motions. In practice, if the range of η is within allowable limits, the final mating is likely to be successful under visual

and manual assistances. The rightmost sketch in Fig. 6 illustrates the outcrossing process of η relative to the circular safety boundary with a radius of R_{sb}. An outcrossing occurs when the tower centre moves across the boundary, and the outcrossing rate is the frequency of outcrossings. The lower the outcrossing rate, the higher success rate of mating. Herein, the critical outcrossing rate, ν_{cr}, is defined as the allowable outcrossing rate for the specified safety boundary. ν_{cr} is often chosen based on engineering experiences, and should be combined with onboard motion measurements to achieve reliable mating. In this paper, we assume that the phase for assembly positioning lasts a maximum of 30 minutes, during which 10 outcrossings are allowable ($\nu_{cr} = 5.5 \cdot 10^{-3}$ Hz). The critical motion radius, η_{cr}, corresponding to ν_{cr} can be derived from motion traces. The mating process will follow, if the critical motion radius, η_{cr} is sufficiently low, as expressed by Eq.(1):

$$\eta_{cr} \leq R_{sb} \tag{1}$$

3. System modelling

3.1. Modelling challenges

There exist challenges to numerically model the entire installation process. The following three points are identified as the major challenges here:

- Structural dynamics. Because multiple bodies including the wind turbines, the catamaran and the moored spar foundation are interconnected via mechanical couplings, the coupled system exhibits a number of eigen modes. It is important to model the mechanical couplings and understand their effects on the dynamic characteristics of the system.

- Hydrodynamics. Hydrodynamic properties of two rigid bodies are involved in the catamaran-spar system, and the hydrodynamic interaction must be considered during the hydrodynamic load calculation. For the catamaran, the sloshing modes between the two monohulls should be captured. For the spar foundation, the second-order hydrodynamic effects may play a bigger role in shallow waters. In addition, viscous effects on the catamaran and spar should be considered in the modelling.

- Automatic control. For different stages of the installation process, demands arise for automatic control of various components of the system. For the phase when the relative motion is being monitored (step 6), the focus is on the dynamic positioning of the catamaran. For the mating

phase of the wind turbine assembly (step 7), control of the lifting grippers compensating for heave motion of the catamaran should be addressed as well. Moreover, it could be relevant to design a control scheme for the active ballast system of the spar foundation to avoid a sudden change in the draft after mating.

3.2. Modelling methods and tools

The present system was modelled using the features available in SIMO [36]. SIMO is a time-domain simulation program for simulating motions and station keeping of multibody systems. The catamaran installation vessel and the spar foundation are modelled as two rigid bodies connected by mechanical and hydrodynamic couplings between their interfaces. In this initial study, all wind turbine assemblies on board are considered to be rigidly connected to the catamaran. Mooring system and thrusters were added to the spar and the catamaran, respectively. Additionally, HydroD [37] and HAWC2 [5] were used to estimate hydrodynamic properties of the spar and catamaran, and wind coefficients of the wind turbines, respectively.

3.2.1. Hydrodynamic loads modelling

The added mass and potential damping were calculated in the frequency domain, and then applied in the time domain for the coupled motion analysis of two bodies through retardation functions. Fig. 7 displays the panel models developed for the two-body hydrodynamic analysis. Quadrilateral elements were used with an average size of 2 m. For the catamaran, large negative added mass in sway and roll motions were observed close to the lowest natural frequency (0.16 Hz) for antisymmetric sloshing modes between the two hulls [38]. The first- and second-order hydrodynamics were calculated using the potential theory [39]. Fig. 8 shows the heave and pitch response amplitude operators of the free floating bodies for two headings, and the resonant peaks corresponding to the natural periods can be identified: the heave natural periods of the catamaran and the spar are close to 6.5 s and 17.5 s, and the pitch natural periods of the catamaran and the spar are close to 9.1 s and 30 s, respectively. Note that the pitch natural period of the spar will change considerably when the two bodies are connected. The second-order loads in surge, sway, and yaw were calculated based on Newman's approximation; only the difference-frequency part was considered. The viscous forces on the catamaran hull are represented by linear roll damping and quadratic yaw damping coefficients.

For the submerged part of the spar foundation, additional viscous forces should be accounted for. The viscous force on each discrete strip can be expressed by the Morison-type drag formulation:

$$f_s = \frac{1}{2}\rho C_D D(\dot{x}_w - \dot{\eta}_1)|\dot{x}_w - \dot{\eta}_1| \tag{2}$$

where ρ is the density of sea water, and C_D is the quadratic drag coefficient. D is the diameter of each strip, and $\dot{x}_w$ is the velocity of water particle at the strip center. $\dot{\eta}_1$ denotes the velocity of each strip. The drag coefficient is dependent on KC number, Reynolds number, and surface roughness [40]. In this work, the nominal viscous coefficient of 0.9 was applied for the transversal direction.

3.2.2. Aerodynamic forces

In SIMO, the wind field is assumed to be propagating parallel to the horizontal plane, and the varying part of the wind velocity in the mean direction is described by the ISO 19901-1 wind spectrum expressed by Eqs. (3)–(4), where $S(f)$ is the spectral density at frequency f; z is the height above sea level; U_0 is the 1-hour mean wind speed at the 10-m height; n=0.468 [36].

$$S(f) = \frac{320 \cdot (\frac{U_0}{10})^2 \cdot (\frac{z}{10})^{0.45}}{(1 + {f_m}^n)^{5/(3n)}} \tag{3}$$

$$f_m = 172 \cdot f \cdot (\frac{z}{10})^{2/3} \cdot (\frac{U_0}{10})^{-0.75} \tag{4}$$

The wind speed variation along the height is described by the wind profile:

$$\bar{u}(z) = \bar{u}_r(\frac{z}{z_r})^{\psi} \tag{5}$$

where $\bar{u}$ is the average velocity at height z; $\bar{u}_r$ is the average velocity at the reference height z_r above sea level, and ψ is the height coefficient. ψ is set as 0.11 here.

The aerodynamic forces are calculated based on the instantaneous wind and body velocities. For the jth degree of freedom, the force on a body is calculated by the following formula

$$q_j = C_j(\theta)v_{rel}^2 \tag{6}$$

where C_j denotes the wind force coefficient for the instantaneous relative direction, θ is the relative velocity direction in local coordinate system, and v_{rel} is the relative wind speed seen by the body.

In this study, only the aerodynamic forces from the parked wind turbines on deck were considered. The wind coefficients were calculated using HAWC2, a state-of-the-art aeroelastic program. The steady aerodynamic lift and drag coefficients were used to determine the wind loads

on each blade section. In addition, the wind-induced drag on the towers was also considered. For nonrotating turbines, the aerodynamic loading is similar, and the wake effects on the downwind turbines were not considerd. When the catamaran is fully loaded, four DTU 10 MW wind turbines [41] are assumed to be standing still on the deck. Fig. 9 shows the two blade orientations considered. Either orientation may be adopted during offshore transport. The wind direction increases anticlockwise. When the wind is in the x-direction, 0-deg blade pitch gives large drag-dominated loads. The wind coefficients are the forces and moments at the tower bottom for the unit wind speed. Figs. 10(a)–11(b) present variations of the force and moment coefficients with wind direction. When the wind direction is parallel to the x-axis (0 or 180 deg), the catamaran may experience less wind loads if the blade pitch are kept at 90 deg. However, when the wind direction is more aligned with the y-axis (90 or 270 deg), a blade pitch of 0 deg may be preferable.

3.2.3. Mechanical couplings

The sliding grippers are mounted along an arc on the inside of the catamaran's aft. They are designed to grasp the floating foundation and constrain the relative motions in the xy-plane. In the z-direction, there will be sliding movement because of the passive roller at the end tip of each gripper. In the original design of the sliding grippers, the grippers act at three discrete contact points between the spar and the catamaran, as shown in Fig. 4(a). In SIMO, the grippers are numerically modelled as a continuous docking cone device surrounding the spar circumference; see Fig. 12. A docking cone is a spring-damper system with a specified relation between relative radial offset and radial restoring force. Modelling details of the docking cone can be also found in [19, 42]. The docking cone properties will affect the natural periods of the coupled system [43]. A representative docking cone based on the original sliding gripper design with high stiffness was adopted. As shown in Fig. 13, no pretension is applied, and the linear stiffness constant is 1E5 kN/m when the relative displacement exceeds 0.01 m. In addition, a linear damping coefficient of 0.02 kNs/m was used. This small amount of damping was selected for the sake of improved numerical stability, and will not affect vertical motions of the catamaran or the spar foundation.

3.2.4. Positioning system

Fig. 14 shows the configuration of the catenary mooring lines for the spar-type floating wind turbine. Detailed properties of the mooring lines are listed in Table 2. The bridle formed by the

Table 2: Selected properties of the mooring system under no environmental loads

Parameter	*Symbol*	*Value*
Total length of mooring line (m)	L_{moor}	680
Length of upper line (m)	L_{upper}	50
Length of lower line (m)	L_{lower}	630
Diameter of upper chain (mm)	D_{upper}	132
Diameter of lower chain (mm)	D_{lower}	147
Unit submerged weight of upper chain (kN/m)	W_{upper}	3.686
Unit submerged weight of lower chain (kN/m)	W_{lower}	4.240
Product of elastic modulus and cross sectional area of upper chain (kN)	EA_{upper}	1.373E6
Product of elastic modulus and cross sectional area of lower chain (kN)	EA_{lower}	1.682E6
Breaking strength of upper chain (kN)	$T_{b,upper}$	1.299E4
Breaking strength of lower chain (kN)	$T_{b,lower}$	1.553E4
Pretension in the top segment (kN)	T_0	674

delta lines provides large yaw stiffness. The mooring system was modelled by three catenary lines without delta lines. Fig. 15 presents the restoring characterstics of the three mooring lines in two directions. As expected, when offset increases, the restoring curve has steeper slope in the global x-direction (in-line mooring lines) than in the global y-direction (in-between mooring lines). To represent the large yaw stiffness from the delta lines, equivalent hydrostatic stiffness in yaw (2.9E5 kNm/rad) are exerted on the spar. The mooring line model in SIMO combines quasistatic analysis and a simplified method for dynamic tension [44]. This mooring line model is deemed adequate for the present analysis with a focus on motion responses, but may underestimate the tensions in conditions with strong dynamics.

The DP of the catamaran is achieved by regulating four thrusters. The catamaran motion follows the reference point, which is placed at the body origin of the spar. A Kalman filter-based controller is used for the DP system. In the Kalman filter, the mathematical model of the vessel consists of a high frequency mode, a low frequency model, and a model for slowly varying forces from waves and current. The input data to the Kalman filter routines include reference coordinate of the catamaran and the spar, body masses, quadratic drag coefficients, and Kalman filter gain matrix. Vessel motions and environmental forces from wind, waves, and current are estimated. At

each time step, measured forces and positions of the catamaran are used as inputs to the routine, and state variables in the estimator are updated. The thrust demand is computed as feedback from the low frequency state variables and feedforward from measured wind forces and estimated wave and current forces. Detailed descriptions of the Kalman filter model can be found in [45]. Tuning of the controller gains was conducted following a standard procedure [36].

3.2.5. Equations of motion

The coupled catamaran-spar system includes 12 degrees of freedom (DOFs) of rigid body motions. The equations of motion in the time domain are as follows

$$(\boldsymbol{M} + \boldsymbol{A}(\infty))\ddot{\boldsymbol{x}} + \boldsymbol{D_1}\dot{\boldsymbol{x}} + \boldsymbol{D_2}f(\dot{\boldsymbol{x}}) + \boldsymbol{K}\boldsymbol{x} + \int_0^t \boldsymbol{h}(t-\tau)\dot{\boldsymbol{x}}(\tau)d\tau = \boldsymbol{q}(t, \boldsymbol{x}, \dot{\boldsymbol{x}}) \tag{7}$$

where $\boldsymbol{M}$ is the total mass matrix of the catamaran and the spar;

$\boldsymbol{x}$ is the rigid body motion vector with 12 DOFs;

$\boldsymbol{A}$ is the frequency-dependent added mass matrix;

$\boldsymbol{D_1}$ is the linear damping matrix;

$\boldsymbol{D_2}$ is the quadratic damping matrix;

$\boldsymbol{K}$ is the coupled stiffness matrix, which includes the hydrostatic stiffness of the catamaran and the spar, the stiffness from mooring lines, and the mechanical coupling between the catamaran and the spar;

$\boldsymbol{h}$ is the coupled retardation function of the catamaran and the spar, calculated from the frequency-dependent added mass or potential damping;

$\boldsymbol{q}$ is the external force vector that includes the 1st and 2nd order wave excitation forces on the catamaran and the spar, the hydrodynamic viscous force on the two bodies, the wind forces and the station-keeping forces on the catamaran.

3.2.6. Eigen value analysis

To evaluate the eigen properties of the rigid body motions of the coupled system, eigen value analysis was performed in the frequency domain, without the effect of DP. The eigen modes and natural periods were obtained by solving Eq. (8):

$$[-\omega^2(M + A) + C] \cdot X = 0 \tag{8}$$

where ω is the natural frequency, and M is the mass matrix of the catamaran and spar foundation. A is the added mass matrix, and C is the total restoring stiffness matrix, which is split into

hydrostatic restoring, mooring restoring, and coupling between the catamaran and spar. X is the eigenvector that represents rigid body motions, with 6 DOFs for the catamaran and 6 DOFs for the spar.

Table 3 summarises the natural periods and eigen modes of the catamaran and spar. The spar exhibits two dominant modes in roll and pitch. The lower natural period is near one second (s), which is due to high stiffness of the docking cone, and the higher period is close to 40 s. The natural periods of the catamaran in heave, roll, and pitch are below 10 s, which indicate small motions in short waves and larger motions when wave periods are close to the natural periods. Except for the heave (mode No. 7) and yaw (mode No. 5) of the spar, the other eigen modes are coupled.

Table 3: Natural periods and eigenvectors of rigid body motions of the coupled system

Body	Mode	Unit	1	2	3	4	5	6	7	8	9	10	11	12
Catamaran	surge	m	-0.03	-0.38	-0.13	0.28	0.00	0.00	0.00	0.07	-0.29	0.32	0.16	**1.00**
Catamaran	sway	m	0.14	-0.02	0.00	-0.01	0.00	-0.22	0.00	0.41	-0.23	-0.21	0.93	-0.20
Catamaran	heave	m	0.00	-0.03	**-1.00**	-0.07	0.00	0.00	0.00	0.00	0.00	0.00	0.00	0.00
Catamaran	roll	deg	0.07	-0.01	0.00	-0.01	0.00	**-1.00**	0.00	0.05	0.01	0.01	-0.01	0.00
Catamaran	pitch	deg	0.01	0.17	0.46	**-1.00**	0.00	0.00	0.00	0.00	-0.01	0.01	0.00	0.00
Catamaran	yaw	deg	-0.55	0.01	0.00	-0.01	0.00	-0.12	0.00	**1.00**	0.11	0.05	-0.06	-0.12
Spar	surge	m	0.07	0.97	-0.13	0.29	0.00	0.00	0.00	0.12	-0.28	0.32	0.15	0.99
Spar	sway	m	-0.97	0.07	0.00	0.01	0.00	-0.08	0.00	-0.78	-0.36	-0.26	**1.00**	-0.06
Spar	heave	m	0.00	0.00	0.00	0.00	0.00	0.00	**1.00**	0.00	0.00	0.00	0.00	0.00
Spar	roll	deg	**1.00**	-0.07	0.00	-0.01	0.00	0.08	0.00	0.71	**1.00**	0.81	0.07	0.00
Spar	pitch	deg	0.07	**1.00**	-0.14	0.31	0.00	-0.01	0.00	0.11	-0.79	**1.00**	-0.01	0.02
Spar	yaw	deg	0.00	0.00	0.00	0.00	**-1.00**	0.00	0.00	0.00	0.01	0.01	0.00	0.00
Natural	period	s	0.92	1.05	6.72	7.91	8.05	9.09	17.40	22.70	40.56	41.55	86.86	99.27

4. Simulation and results

4.1. Simulation setting

The aim is to investigate the performance of this installation concept under wind and wave conditions. The "Norway 5" site was selected as as a potential site for offshore wind farm. This site is situated in the North Sea and represents generic water depths of 100 m and 200 m [46]. The selected environmental conditions are listed in Table 4. Here, *EC* stands for environmental

condition. H_s is the significant wave height. T_p is the wave peak period. U_w refers to the 1-hour averaged wind speed reported for 10-m height. For the cases with wind, the selected wind speed has high probability of occurrence for a given wave height, based on scatter diagrams of the site. β is the wave heading, which is aligned with the x-axis for β=0 deg, see Fig. 14. Wind and waves are collinear in all cases. α is the blade pitch angle. In the directional short-crested wave spectrum, a constant n of 3 was used in the directional function, $D(\theta)$ [47]. Irregular waves were generated using the JONSWAP spectrum with a peak enhancement factor γ of 3.3 [47]. A water depth of 110 m was considered. For each combination of H_s, T_p, β, U_w, and α in Table 4, six 1800-s simulations with random seeds were conducted, and the statistical results were based on an average of six simulations.

Table 4: Environmental conditions in the study

EC	H_s [m]	T_p [s]	β [deg]	U_w [m/s]	α [deg]
1	1.0	4, 6, 8, 10, 12	0, 30	0, 5.0	0, 90
2	1.5	4, 6, 8, 10, 12	0, 30	0, 7.0	0, 90
3	2.0	4, 6, 8, 10, 12	0, 30	0, 8.0	0, 90
4	2.5	4, 6, 8, 10, 12	0, 30	0, 10.0	0, 90
5	3.0	4, 6, 8, 10, 12	0, 30	0, 11.0	0, 90

4.2. Motion comparison

The motion responses of the catamaran and spar all refer to the body coordinate systems, the origins given by Table 1. Note that the spar's body origin coincides with the global origin in the beginning of simulations.

4.2.1. Catamaran motion

The motion reference point of the catamaran lies on the water plane midship. Figs. 16 shows selected time series of the catamaran pitch and surge motions for a representative sea state (H_s=2.5 m, T_p=12 s, β=0 deg). Compared to the wave-only condition, the addition of wind loads from the blade pitch=90 deg amplifies the range of the surge motion. In contrast, the wind effect on the pitch motion is limited; even the blade pitch=0 deg conditions with considerable wind drag induce small differences.

Figs. 17(a)–17(d) display selected response spectra for EC 4 with H_s=2.5 m and T_p=12 s. The surge, heave, and pitch motions are compared for β=0 deg, and the roll motion for β=30 deg. The

surge motion is dominated by the resonant response at low frequency. As shown by Fig. 17(a), although the wind loads for blade pitch=90 deg are limited, an increase in the surge resonant peak is clearly observed. For blade pitch=0 deg, a more peaked surge resonance (spectral density=116 m^2s/rad) is found and not shown. Interestingly, the second pitch mode of the spar is observed, because of the motion coupling of the floating bodies in surge. The heave, pitch, and roll motion responses of the catamaran are dominated by the wave frequency, which is not affected by the wind loads. In Fig. 17(c), a small pitch resonant peak can be found near ω=0.86 rad/s. Addition of the wind loads will create a moment on the catamaran, and the magnitude of this peak increases more for blade pitch=0 deg.

Figs. 18(a)–18(d) show variation of the catamaran's surge and pitch standard deviations (STDs) with H_s and T_p. In general, the surge STD is less sensitive to T_p than the pitch STD which has greater values near T_p=12 s (Fig. 18(c)). This observation appears, because the surge motion is governed by the low-frequency response, whereas the pitch motion dominated by the wave-frequency response. The wave-frequency response relates to the shape of the wave spectrum and the pitch response amplitude operator, because STD is equal to the integrated area of a given response spectrum. Although T_p=12 s is away from the pitch natural period of the catamaran (T_{n5}=7.91 s), the integrated area of the pitch spectrum still exceeds those at lower T_p. As clearly shown by Figs. 18(b) and 18(d), an increase in H_s causes greater surge and pitch STD, which is reasonable. The motion response spectra in Fig. 17 can be used to elucidate the differences in STD. Take the wave-only cases as the reference. For H_s=2.5 m and varying T_p, the cases with blade pitch=90 deg exceed the reference by 26% in the surge STD and 0.5% in the pitch STD, and the cases with blade pitch=0 deg by more than 100% in the surge STD and 7% in the pitch STD on average. The negligible differences in the pitch STD are due to the limited contribution of the pitch resonant peak to the spectrum (Fig. 17(c)).

4.2.2. Spar motion

The motion reference point of the spar foundation lies on the centreline of the platform and is at mean water level. Figs. 19 shows representative time series of the spar pitch and surge motions. Because the spar and the catamaran are connected by mechanical coupling, the surge responses of them are similar at the motion reference point, and the presence of wind force has an impact on the spar surge motion as well. Unlike the catamaran, the spar pitch motion is more sensitive to the wind effect. In the time series shown, the maximum spar pitch motion exceeds 4 deg when

blade pitch=0 deg.

Because of tight coupling between the catamaran and the spar in the horizontal plane, the surge spectrum of the spar is similarly dominated by the low-frequency peak, as shown by Fig. 20(a). Addition of wind loads will further amplify this peak. As mentioned above, the heave motion of the spar is uncoupled, and the spectrum is dominated by the heave resonance (Fig. 20(b)). With or without the presence of wind forces, the heave response spectrum remains the same. The surge and pitch motions of the spar are coupled, and the second pitch mode (near 0.15 rad/s) of the spar can be found, in addition to the wave frequency. The pitch motion of the spar is dominated by the second pitch mode, unlike that of the catamaran. When considerable wind loads are exerted on the catamaran for blade pitch=0 deg, the increased surge motions cause greater pitch motions. In contrast, the wave-frequency response is less significant. As indicated by Fig. 20(d), the spectral density of the roll motion has low magnitude in oblique waves at β=30 deg. The wave-frequency response is dominant in the spectrum, and the low-frequency peak because of the sway response can be observed near 0.06 rad/s. This peak is slightly affected by the wind, but the effect on the roll STD is limited.

Figs. 21(a)–21(d) show the surge and pitch motion STD of the spar. For the surge STD, the trend of variation with H_s or T_p is very similar to that of the catamaran, and the cases with more wind loads (blade pitch=0 deg) consistently experience greater STD. For the pitch STD, larger values are also reported for higher T_p and H_s. It is worthy of note that, the pitch STD of the spar is more sensitive to the wind loads than that of the catamaran. For the spar foundation, the distance between its COG and the sliding grippers exceeds 50 m, and the fluctuating horizontal forces provided by the grippers lead to rotational moments about the COG. Thus, the increases in the surge STD of the spar due to wind loads directly affect the pitch STD of the spar. For H_s=2.5 m and varying T_p, and compared to the reference cases with waves only, the cases with blade pitch=90 deg exceed by 6% in the pitch STD, and the cases with blade pitch=0 deg exceed by 51% on average. For both cases, appreciable differences in pitch STD are found at lower T_p. When T_p increases to 12 s, the difference is only 0.1% for blade pitch=90 deg, and 6.5% for blade pitch=0 deg, see Fig. 21(c).

4.2.3. Relative motion at the mating point

As shown in Fig. 14, the mating point is atop the spar foundation, 20 m above the waterline. After weight shift of the wind turbine assembly, this point will sink by 10 m. According to the principle

of rigid body motion, the motions of the mating point in three directions can be calculated by Eq. (9) in the case of small rotated motions:

$$\hat{s} = (s_1 + z_r s_5 - y_r s_6)\hat{i} + (s_2 - z_r s_4 + x_r s_6)\hat{j} + (s_3 + y_r s_4 - x_r s_5)\hat{k} \tag{9}$$

where s_1 to s_6 are the rigid body motions of the catamaran or the spar, and (x_r, y_r, z_r) is the position of the mating point relative to the body origin. The lifting grippers were not modelled, so Eq. (9) was applied to both bodies.

Fig. 22(a) shows the motion traces of the mating point in the xy-plane. As the catamaran and spar are following the seas, the relative surge is governing and the maximum value can exceed 2 m in the case. The relative surge is affected by the pitch motion of the spar. As identified in Fig. 22(b), the first-order motions induced by waves contribute most to the relative surge STD, and the second-order effect of the mean drift does not affect the relative motion responses. When wind loads are present, only the peak corresponding to the second pitch natural frequency of the spar is amplified, see the blue dash-dot line. Based on the time series of the relative motion in two directions, the relative motion radius, η, is compared in Fig. 22(c) for a 600-s simulation. The local maxima are dominated by the condition with blade pitch=0 deg. Fig. 22(d) shows the relation between the outcrossing rate and the relative motion radius, defined in Section 2.3. The marked red points are the interpolated critical motion radius, η_{cr}, based on ν_{cr}. The difference in η_{cr} between the two points is less than 5%.

Figs. 23(a)– 23(b) demonstrate sensitivity of the relative surge STD to H_s, T_p, and wind conditions. When T_p or H_s increases, so does the STD. The trend for H_s was observed in previous sections, because of the correlation between the first-order motions and wave height. The trend for T_p is not similarly found in the surge STD of the catamaran (Fig. 18(a)) or the spar (Fig. 21(a)), because these absolute surge STDs are governed by the low-frequency responses and are sensitive to the wind conditions, as indicated by Fig. 17(a) and Fig. 20(a), whereas the relative surge STD is governed by the wave-frequency responses and is less influenced by the wind conditions; see Fig. 22(b).

Table 5 summarises η_{cr} under two wave headings and various wind-wave conditions. H_s has a heavy impact on η_{cr}, which increases by an average of 40% for every 0.5-m increment in H_s. Because the relative surge motion affects η_{cr} more, an increase in the wave heading, β, causes a reduction of approximately 10% in η_{cr}. Still, the effect of wind is limited. For blade pitch=0 deg, the relative increase in η_{cr} remains within 6%, compared against the wave-only case. For blade pitch=90 deg,

Table 5: Estimation of the critical relative motion radius, η_{cr}, of the mating point, T_p=12 s

EC	H_s (m)	$\beta = 0$ deg			$\beta = 30$ deg		
		wave-only	wind-wave[1]	wind-wave[2]	wave-only	wind-wave[1]	wind-wave[2]
1	1	0.53	0.53	0.54	0.49	0.49	0.49
2	1.5	0.84	0.83	0.85	0.76	0.76	0.78
3	2	1.15	1.17	1.20	1.05	1.06	1.09
4	2.5	1.51	1.56	1.62	1.38	1.39	1.45
5	3	1.93	1.98	2.09	1.74	1.74	1.85

[1] blade pitch=90 deg

[2] blade pitch=0 deg

the relative increase is negligible. Overall, the estimated critical relative motion radius is less than 2.1 m in all sea states considered. R_{sb} is dependent on the configuration of the cursor system. If R_{sb} is equivalent to 2.0 m, Eq.(1) is easily satisfied for H_s below 2.5 m. Judging by this criteria, the motion performance of this concept is satisfactory during positioning of a wind turbine assembly.

4.3. Forces on the sliding grippers

Fig. 24 presents a short time history of the gripper forces under the wave-only cases. According to the sensitivity study performed, the magnitude of the gripper force is related to both the docking cone stiffness and the external loading. In this case, a relatively high stiffness of 1E5 kN/m is used, and the two pitch or roll natural periods of the spar are away from the wave periods; see Table 3. Even so, a high-frequency component (approximately 1 Hz) associated with the lower pitch or roll natural periods can be found in the force components. For the two wave headings and the two force components considered, the x-component of the gripper force is dominant. Because of the wave spreading, considerable y-component exists for 0-deg wave heading.

In the following, only the total force is discussed. As shown in Figs. 25(a)– 25(b), the trend of variation of the gripper force STD relative to H_s and T_p is similar to that of the relative motion. For a docking cone with linear stiffness, the gripper force STD is proportional to the relative displacement at the gripper location. Among the three wind-wave conditions, there is limited difference in the STD, which is driven by the first-order motions. The effect of wave heading is shown in Figs. 25(c)– 25(d). On average, β=30 deg causes a 13% and 18% reduction in the force

STD and maximum, respectively. The gripper force is provided by three hydraulic actuators [29], which must be designed to withstand this load range (400 tonnes each).

4.4. Mooring line tension

Amongst the three mooring lines, lines 2 and 3 experience greater loads than line 1, which is intuitive given the mooring layout and wave headings (Fig. 14). The top tension in line 2 at β=0 deg is analysed here. Fig. 26 presents the dynamic part of the top tension in three conditions, from which both low- and high-frequency oscillations can be observed. When blade pitch=0 deg, the amplitude of the low-frequency cycles is substantially increased. As shown in Fig. 27(a), the low-frequency surge motion dominates the tension response, and the addition of wind loads enhances this peak. Moreover, because of the heave motion of the spar foundation, a smaller peak corresponding to the heave natural frequency can be observed, too. Fig. 27(b) shows the trend of variation of the tension STD with regard to H_s. A 40–60% increase in STD is found when H_s rises by 0.5 m. Compared to the wave-only cases, the wave-wind cases can result in a substantial increase greater than 100% when blade pitch=0 deg. Still, the difference in STD becomes insignificant when the maximum tension is concerned (close to 1000 kN).

The mooring line design should take into account both the ultimate strength and fatigue lifetime [48]. Neither is driven by the load cases under operational sea states.

4.5. Section summary

Based on discussions in Sections 4.2–4.4, Table 6 provides general observations of the effect of wave-wind parameters on selected response standard deviations. In the table, U_w represents the effect of wind with blade pitch=0 deg. Vary the values of the environmental parameters listed in Table 4, and if the differences in the simulation results are close to or above 10%, the environmental parameter is deemed important; otherwise not important. Among the environmental parameters, H_s affects all investigated responses and can be regarded as the most important parameter. The relative motion at the mating point in the horizontal plane is critical to the successful mating of wind turbine assembly. It is sensitive to H_s, T_p, and β.

5. Conclusions

This study considers an offshore wind turbine installation concept using a catamaran installation vessel. A numerical model was established involving a catamaran, a spar foundation, mechanical

Table 6: Effect of environmental parameters on selected response variables

Response	Object	H_s	T_p	β	U_w
Surge motion	Catamaran	I	NI	I	I
	Spar	I	NI	I	I
Pitch motion	Catamaran	I	I	I	NI
	Spar	I	I	I	I
Heave motion	Catamaran	I	I	I	NI
	Spar	I	I	NI	NI
Relative motion	Mating point	I	I	I	NI
Force	Grippers	I	I	I	NI
	Mooring line tension	I	NI	I	I

I: important

NI: not important

couplings, mooring lines, and dynamic positioning system. Time-domain simulations were conducted with a focus on the phase when one turbine assembly is being positioned. The main conclusions are as follows:

- From eigen value analysis of the system, most of the mode shapes have a combination of different degrees of freedom. Two pitch and roll modes are present for the spar foundation, because of the mechanical coupling between the bodies. The pitch mode with higher natural period is dominant; it is present in the pitch and surge responses of the spar.

- Two blade orientations with the blade pitch of 90 deg and 0 deg are selected. For the low-frequency surge and the mooring line tension, the 0-deg blade pitch causes a substantial increase in the standard deviation, whereas the 90-deg blade pitch causes a negligible increase. The pitch motion of the spar is more sensitive to the blade orientation. Other motion responses, as well as the gripper forces, are less affected by the blade orientation.

- The relative motion between the wind turbine tower and the spar at the mating point is key to the success of mating. The relative motion radius is used as the metric to evaluate the present concept. This variable is governed by the first-order motions and is sensitive to

the significant wave height and spectral peak period, but insensitive to the wind condition. Under the investigated sea states, the obtained critical motion radius is always below 2.1 m, during a period of 30 minutes.

- Two wave headings, and five levels of significant wave height and spectral peak period are considered. The relative motion radius, and the gripper forces have larger value at 0-deg wave heading than 30-deg wave heading, because the relative surge motion is more important. Greater responses are associated with larger wave heights and peak periods.

6. Limitations and future work

The focus of this paper is on the positioning phase of wind turbine assembly. The lifting grippers were not modelled, as they will not affect the relative motions in the horizontal plane. During the mating phase of the tower bottom with the spar top, the lifting grippers will function to minimise the impact load. The suggested cursor system is not modelled either. These modelling aspects will be pursued in future.

7. Acknowledgements

This work has been financially supported by the Research Council of Norway granted through the Department of Marine Technology and the Centre for Research-based Innovation of Marine Operations (SFI MOVE) at NTNU (RCN project 237929). The first author thanks Karl Erik Kaasen of SINTEF Ocean for discussions.

References

[1] P. Sclavounos, S. Lee, J. DiPietro, G. Potenza, P. Caramuscio, G. De Michele, Floating offshore wind turbines: tension leg platform and taught leg buoy concepts supporting 3-5 mw wind turbines, in: European wind energy conference EWEC, 2010, pp. 20–23.

[2] I. Pineda, P. Tardieu, The european offshore wind industry key trends and statistics 2016, https://windeurope.org/about-wind/statistics/offshore/european-offshore-wind-industry-key-trends-and-statistics-2016/, Accessed: 2017-06-01.

[3] K. E. Steen, Hywind scotland – status and plans, http://www.sintef.no/projectweb/deepwind_2016/presentations/, Accessed: 2017-02-01.

[4] J. M. Jonkman, M. L. Buhl Jr, FAST User's Guide-Updated August 2005, Technical Report, National Renewable Energy Laboratory (NREL), Golden, CO., 2005.

[5] T. J. Larsen, A. M. Hansen, How 2 HAWC2, the User's Manual, Technical Report, Risø National Laboratory, 2007.

[6] E. Bossanyi, GH Bladed User Manual, Technical Report, Garrad Hassan Bladed, 2009.

[7] E. N. Wayman, P. Sclavounos, S. Butterfield, J. Jonkman, W. Musial, et al., Coupled dynamic modeling of floating wind turbine systems, in: Offshore technology conference, Offshore Technology Conference, 2006.

[8] J. M. Jonkman, Dynamics of offshore floating wind turbinesmodel development and verification, Wind energy 12 (2009) 459–492.

[9] Z. Jiang, M. Karimirad, T. Moan, et al., Response analysis of parked spar-type wind turbine considering blade-pitch mechanism fault, International Journal of Offshore and Polar Engineering 23 (2013).

[10] Z. Jiang, M. Karimirad, T. Moan, Dynamic response analysis of wind turbines under blade pitch system fault, grid loss, and shutdown events, Wind Energy 17 (2014) 1385–1409.

[11] Z. Jiang, T. Moan, Z. Gao, A comparative study of shutdown procedures on the dynamic responses of wind turbines, Journal of Offshore Mechanics and Arctic Engineering 137 (2015) 011904.

[12] A. Sarkar, O. T. Gudmestad, Study on a new method for installing a monopile and a fully integrated offshore wind turbine structure, Marine structures 33 (2013) 160–187.

[13] W. G. Acero, Z. Gao, T. Moan, Numerical study of a novel procedure for installing the tower and rotor nacelle assembly of offshore wind turbines based on the inverted pendulum principle , Journal of Marine Science and Application 16 (2017) 243–260.

[14] D. Ahn, S.-c. Shin, S.-y. Kim, H. Kharoufi, H.-c. Kim, Comparative evaluation of different offshore wind turbine installation vessels for korean west–south wind farm, International Journal of Naval Architecture and Ocean Engineering 9 (2017) 45–54.

[15] J. Paterson, F. D'Amico, P. Thies, E. Kurt, G. Harrison, Offshore wind installation vessels–a comparative assessment for uk offshore rounds 1 and 2, Ocean Engineering (2017).

[16] M. Esteban, B. Couñago, J. López-Gutiérrez, V. Negro, F. Vellisco, Gravity based support structures for offshore wind turbine generators: Review of the installation process, Ocean Engineering 110 (2015) 281–291.

[17] M. Collu, A. Maggi, P. Gualeni, C. M. Rizzo, F. Brennan, Stability requirements for floating offshore wind turbine (fowt) during assembly and temporary phases: Overview and application, Ocean Engineering 84 (2014) 164–175.

[18] L. Li, W. G. Acero, Z. Gao, T. Moan, Assessment of allowable sea states during installation of offshore wind turbine monopiles with shallow penetration in the seabed, Journal of Offshore Mechanics and Arctic Engineering 138 (2016) 041902.

[19] L. Li, Z. Gao, T. Moan, H. Ormberg, Analysis of lifting operation of a monopile for an offshore wind turbine considering vessel shielding effects, Marine Structures 39 (2014) 287–314.

[20] L. Li, Z. Gao, T. Moan, Response analysis of a nonstationary lowering operation for an offshore wind turbine monopile substructure, Journal of Offshore Mechanics and Arctic Engineering 137 (2015) 051902.

[21] L. Li, Dynamic analysis of the installation of monopiles for offshore wind turbines (2016).

[22] W. G. Acero, Z. Gao, T. Moan, Methodology for assessment of the allowable sea states during installation of an offshore wind turbine transition piece structure onto a monopile foundation, Journal of Offshore Mechanics and Arctic Engineering 139 (2017) 061901.

[23] K. Thomsen, Offshore wind: a comprehensive guide to successful offshore wind farm installation, Academic Press, 2014.

[24] K. H. lIEN, Hywind scotland – marine operations, `http://www.norcowe.no/doc/konferanser/2016/`, Accessed: 2017-02-01.

[25] N. Ku, M.-I. Roh, Dynamic response simulation of an offshore wind turbine suspended by a floating crane, Ships and Offshore Structures 10 (2015) 621–634.

[26] W. Wang, Y. Bai, Investigation on installation of offshore wind turbines, Journal of Marine Science and Application 9 (2010) 175–180.

[27] a parametric study (????).

[28] S. AS, Hywind installation, https://www.statoil.com/en/how-and-why/innovate/the-hywind-challenge.html, Accessed: 2017-02-01.

[29] L. I. Hatledal, H. Zhang, K. H. Halse, H. P. Hilder, Numerical simulation of novel gripper mechanism between catamaran and turbine foundation for offshore wind turbine installation, in: ASME 2017 36th International Conference on Ocean, Offshore and Arctic Engineering, American Society of Mechanical Engineers, 2017, pp. OMAE2017–62342.

[30] T. G. Monteiro, K. H. Halse, Catamaran for wind turbine installation, stability and response report, Technical Report, Faculty of Maritime Technology and Operations, Norwegian University of Science and Technology, Ålesund, Norway, 2017.

[31] U. A. Korde, Active heave compensation on drill-ships in irregular waves, Ocean Engineering 25 (1998) 541–561.

[32] S. I. Sagatun, T. A. Johansen, T. I. Fossen, F. G. Nielsen, Wave synchronizing crane control during water entry in offshore moonpool operations, in: Control Applications, 2002. Proceedings of the 2002 International Conference on, volume 1, IEEE, 2002, pp. 174–179.

[33] K. Maritime, Motion reference unit, https://www.km.kongsberg.com/ks/web/nokbg0240.nsf/AllWeb/61118F926CD5A6E5C125700B0033CF55?OpenDocument, Accessed: 2017-02-01.

[34] A. B.V., Marine software system - octopus, http://new.abb.com/marine/systems-and-solutions/automation-and-marinesoftware/advisory, Accessed: 2017-02-01.

[35] W. G. Acero, L. Li, Z. Gao, T. Moan, Methodology for assessment of the operational limits and operability of marine operations, Ocean Engineering 125 (2016) 308–327.

[36] MARINTEK, SIMO - Theory Manual Version 4.8.4, 2016.

[37] D. N. Veritas, SESAM user manual HydroD, program version 4.5, 2011.

[38] O. Faltinsen, Sea loads on ships and offshore structures, volume 1, Cambridge university press, 1993.

[39] C. Lee, WAMIT theory manual, Department of Ocean Engineering, Massachusetts Institute of Technology, USA, 1995.

[40] DNV, Recommended Practice DNV-RP-H103, Modelling and Analysis of Marine Operations, 2014.

[41] C. Bak, F. Zahle, R. Bitsche, T. Kim, A. Yde, L. C. Henriksen, M. H. Hansen, J. P. A. A. Blasques, M. Gaunaa, A. Natarajan, The dtu 10-mw reference wind turbine, in: Danish Wind Power Research 2013, 2013.

[42] L. Li, Z. Gao, T. Moan, Numerical simulations for installation of offshore wind turbine monopiles using floating vessels, ASME Paper No. OMAE2013-11200 (2013).

[43] Z. Jiang, Z. Gao, Numerical modelling of the catamaran installation vessel and spar system, Technical Report, Department of Marine Technology, Norwegian University of Science and Technology, Trondheim, Norway, 2017.

[44] K. Larsen, P. C. Sandvik, et al., Efficient methods for the calculation of dynamic mooring line tension, in: The First ISOPE European Offshore Mechanics Symposium, International Society of Offshore and Polar Engineers, 1990.

[45] J. G. Balchen, N. A. Jenssen, E. Mathisen, S. Sælid, A dynamic positioning system based on kalman filtering and optimal control, Modeling, identification and control 1 (1980) 135.

[46] L. Li, Z. Gao, T. Moan, Joint distribution of environmental condition at five european offshore sites for design of combined wind and wave energy devices, Journal of Offshore Mechanics and Arctic Engineering 137 (2015) 031901.

[47] DNV, Recommended Practice DNV-RP-C205, Environmental Conditions and Environmental Loads, 2010.

[48] D. N. Veritas, Offshore standard dnv-os-e301 position mooring, 2008.

[49] P. Brodtkorb, P. Johannesson, G. Lindgren, I. Rychlik, J. Rydén, E. Sjö, WAFO - a Matlab toolbox for the analysis of random waves and loads, in: Proc. 10'th Int. Offshore and Polar Eng. Conf., ISOPE, Seattle, USA, volume 3, 2000, pp. 343–350.

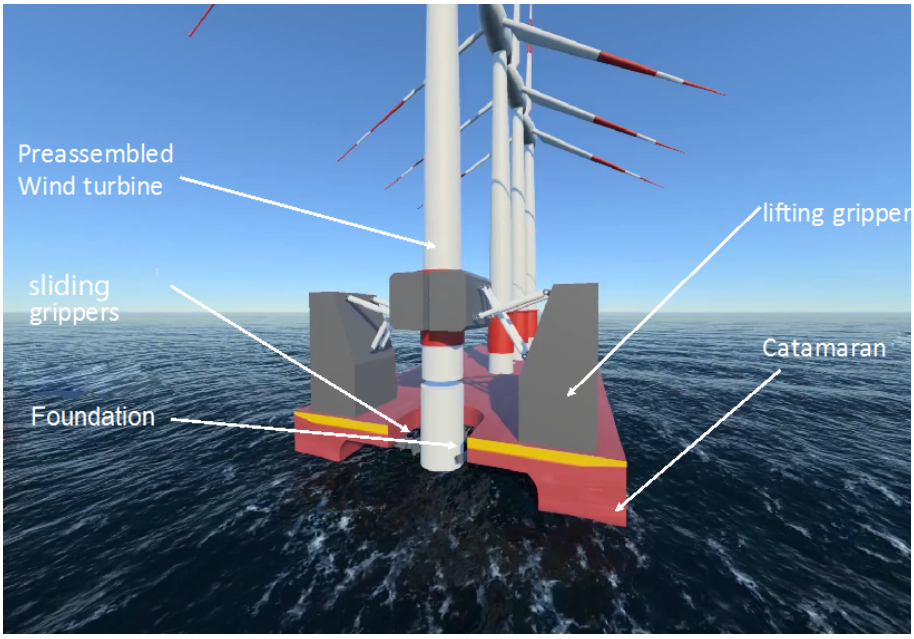

Figure 1: Overview of the catamaran concept during installation of a floating wind turbine.

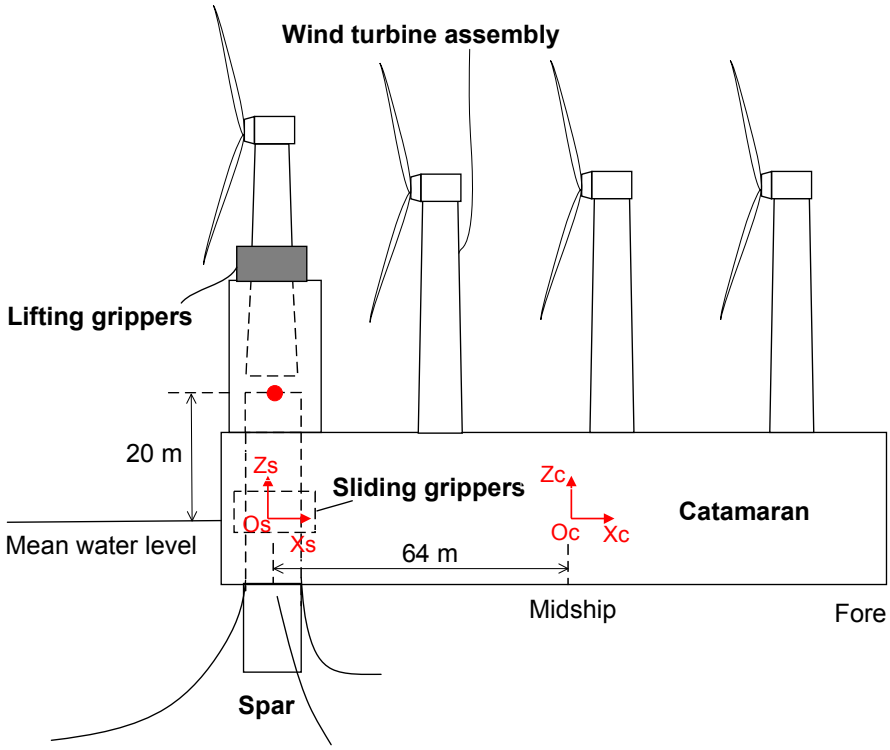

Figure 2: Schematic of the main components involved during a mating operation of the present concept.

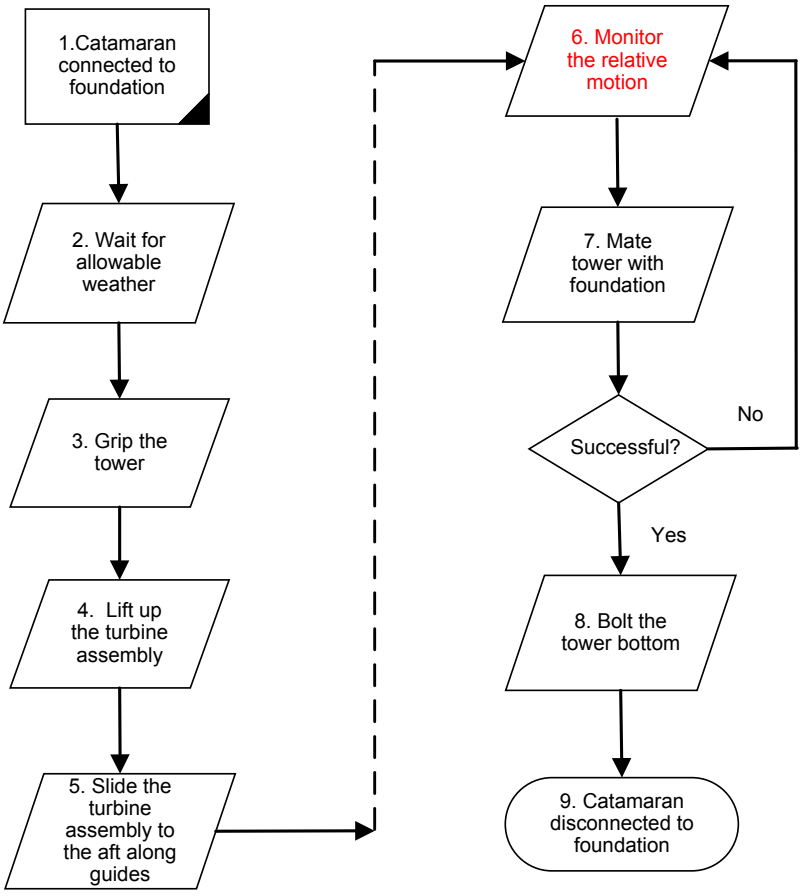

Figure 3: Proposed installation flowchart of the present concept

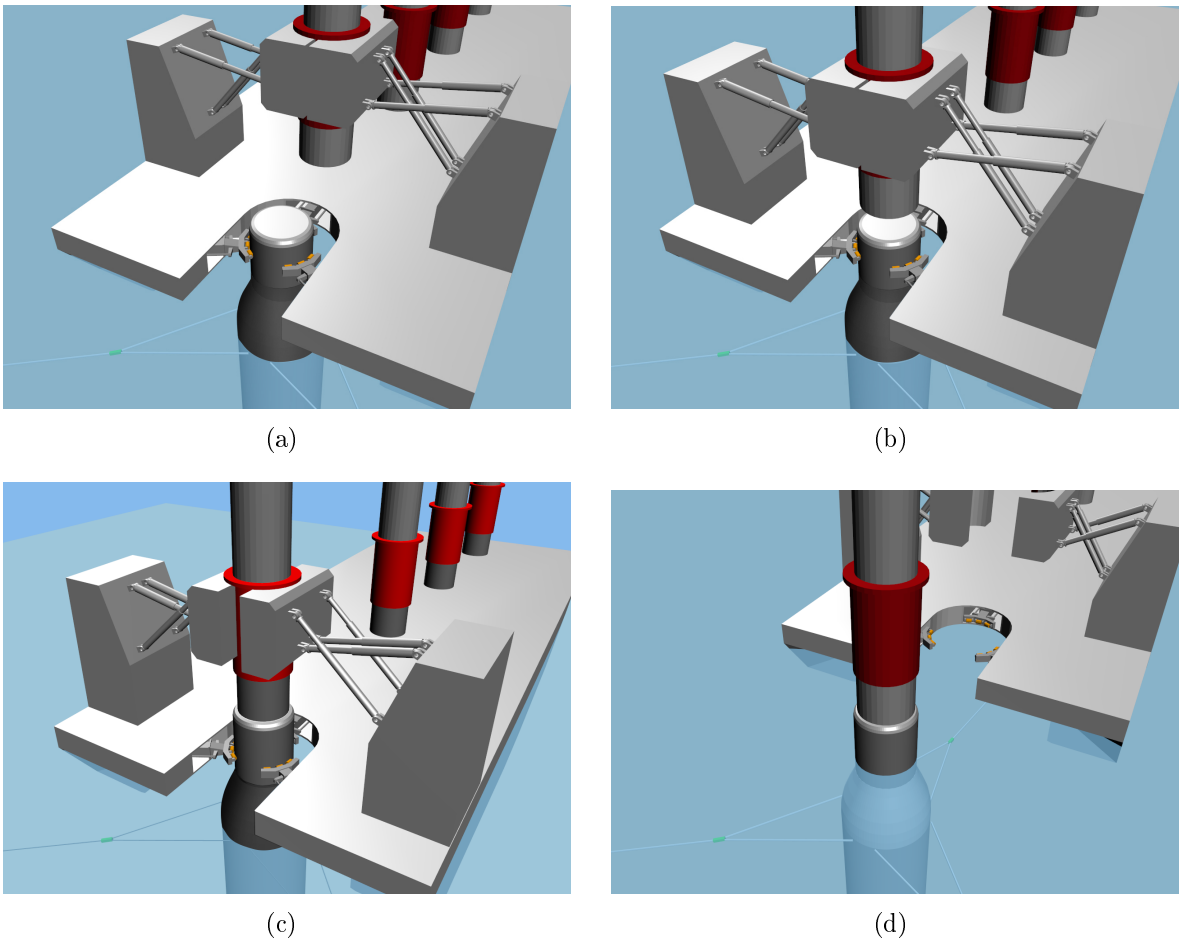

(a) (b)

(c) (d)

Figure 4: Illustration of installation steps: (a) step 5, transferring the turbine assembly; (b) step 6, monitoring the relative motion; (c) step 7, mating the tower bottom; (d) step 9, releasing the spar foundation.

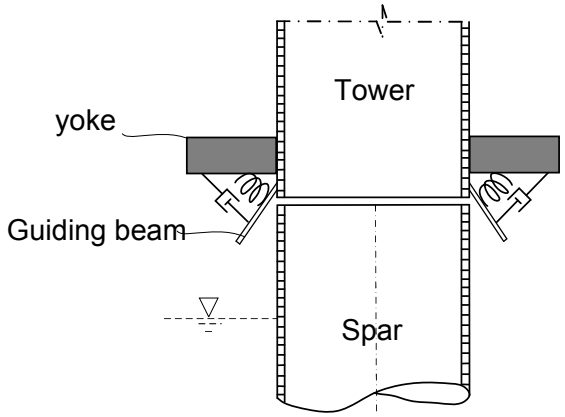

Figure 5: Schematic of the suggested cursor system for mating operation.

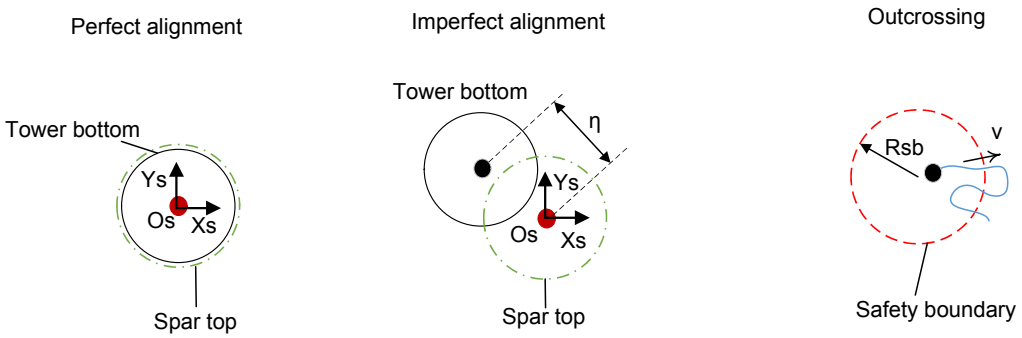

Figure 6: Scenarios of the relative positions between spar top and tower bottom.

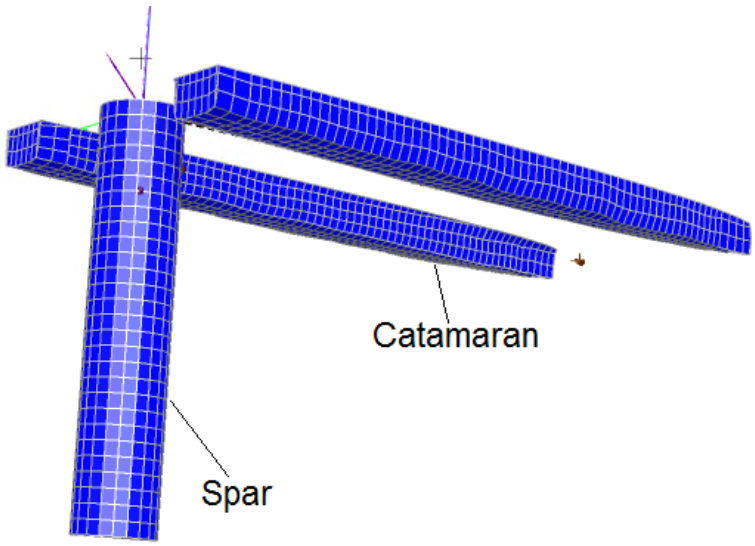

Figure 7: Panel models applied in the hydrodynamic analysis.

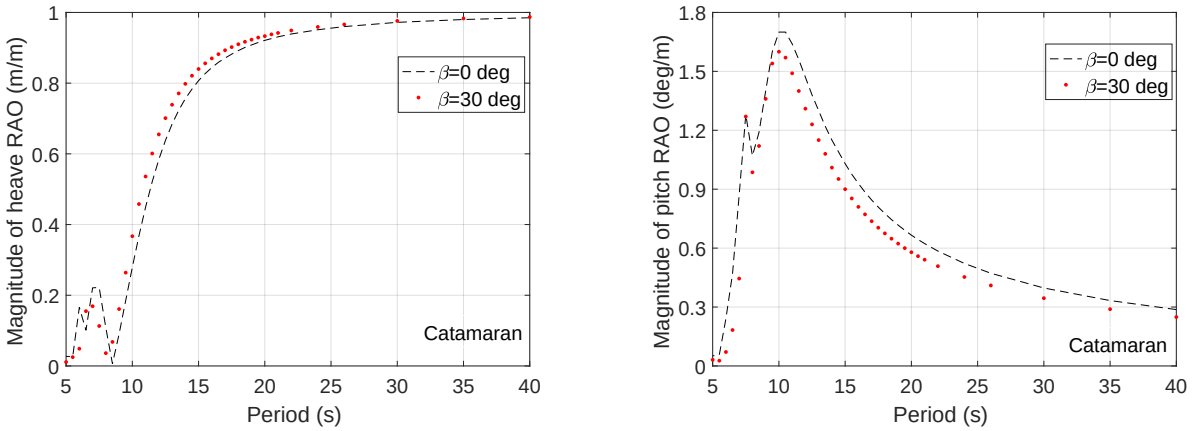

(a)

(b)

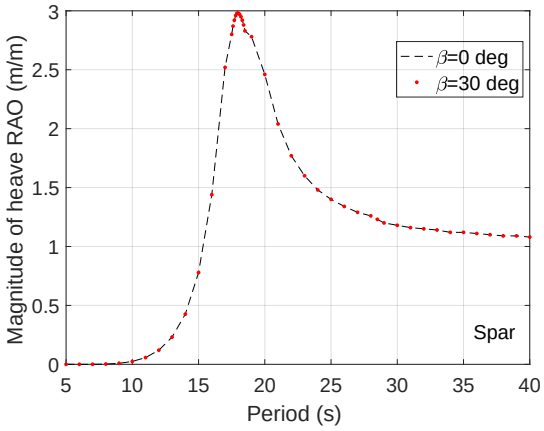

(c)

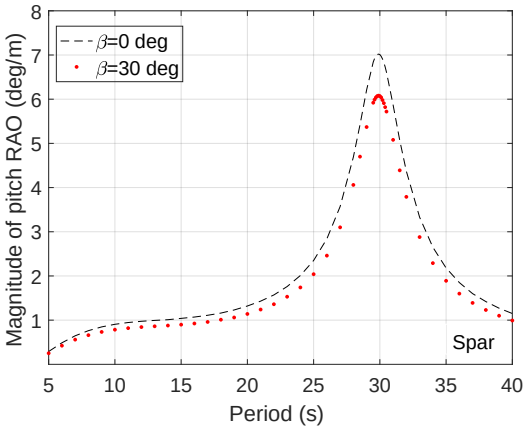

(d)

Figure 8: Selected response amplitude operators (RAOs) of the free-floating bodies (a) heave motion of the catamaran (b) pitch motion of the catamaran; (c) heave motion of the spar foundation; (d) pitch motion of the spar foundation. (β represents wave heading, refer to Fig. 14
)

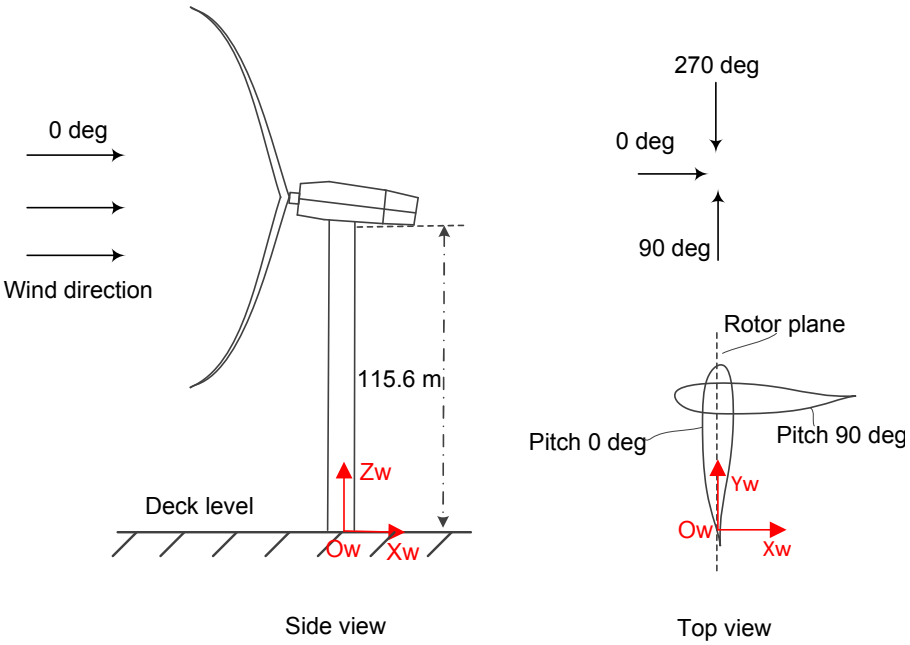

Figure 9: Illustration of the blade orientations and wind directions

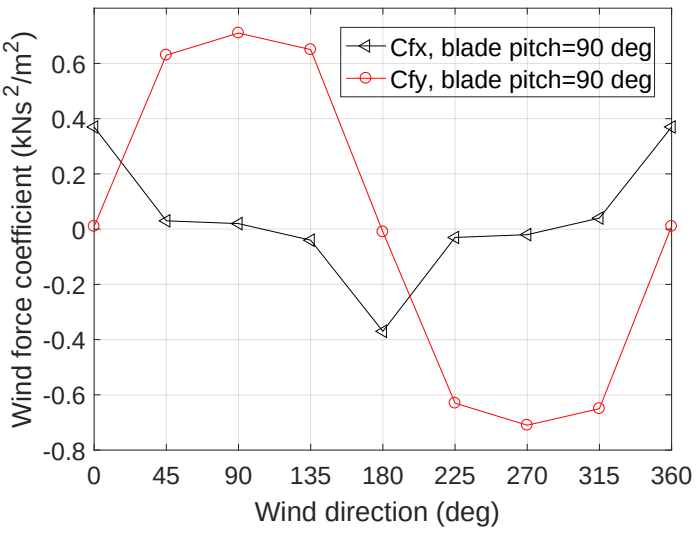

(a)

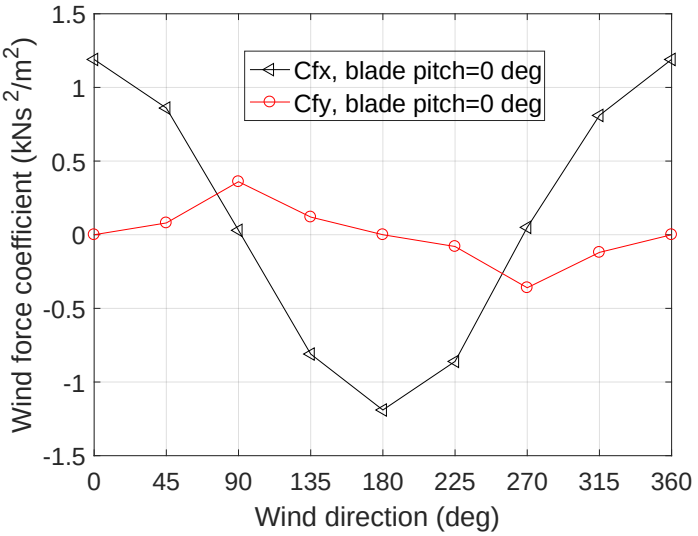

(b)

Figure 10: Wind force coefficients of a single wind turbine: (a) blade pitch=90 deg; (b) blade pitch=0 deg.

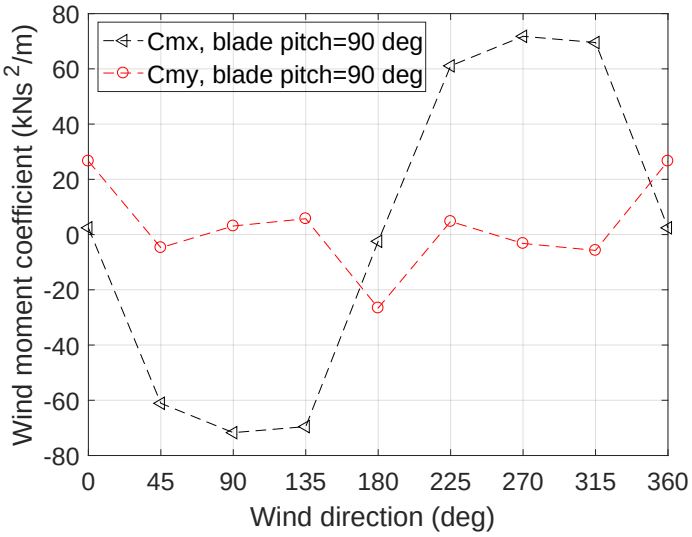

(a)

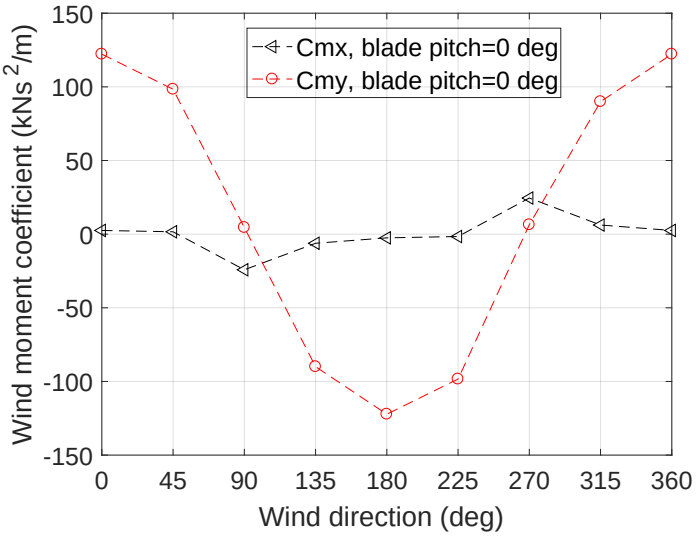

(b)

Figure 11: Wind moment coefficients of a single wind turbine: (a) blade pitch=90 deg; (b) blade pitch=0 deg.

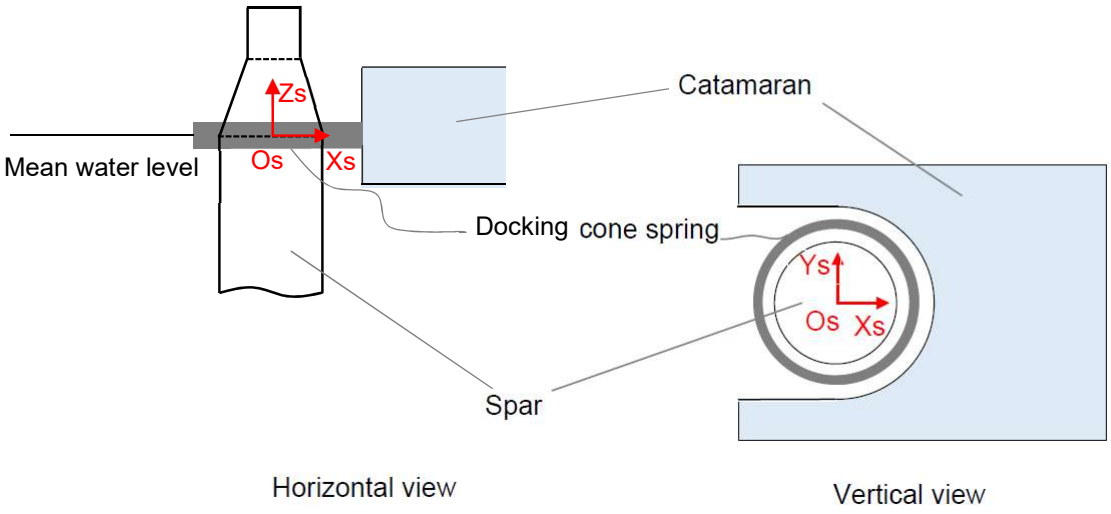

Figure 12: Modelling of the sliding gripper device by a docking cone.

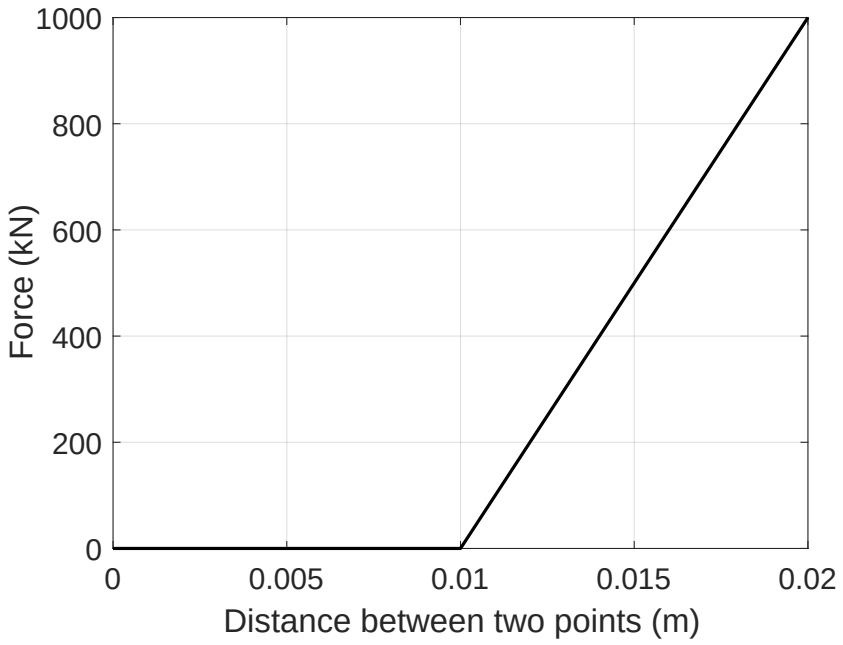

Figure 13: Force-displacement relationship of the applied docking cone.

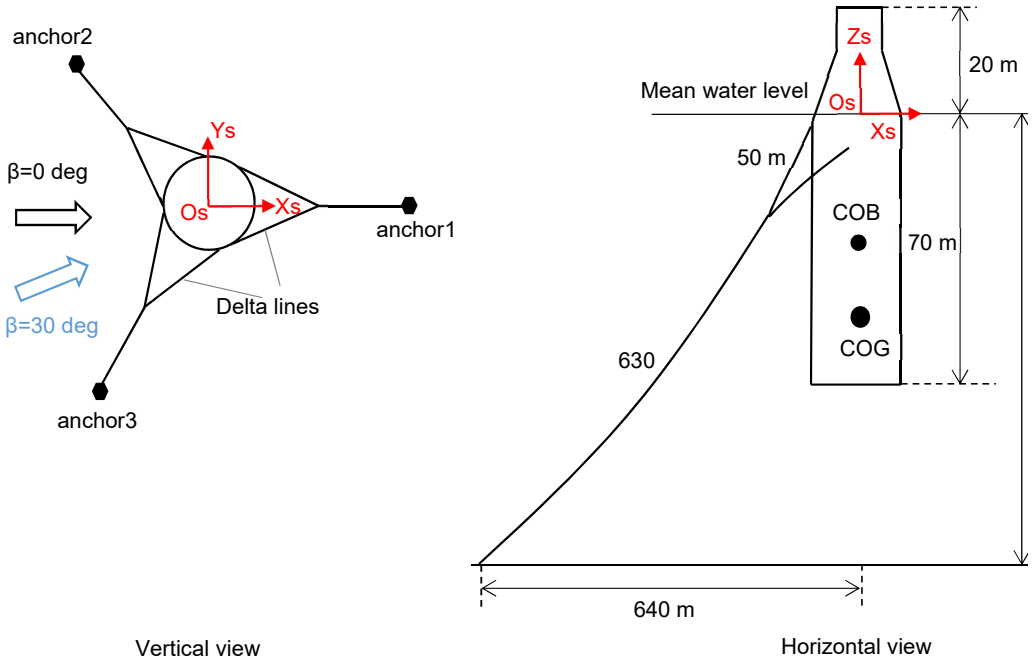

Figure 14: Schematic layout of the mooring system for the floating spar foundation.

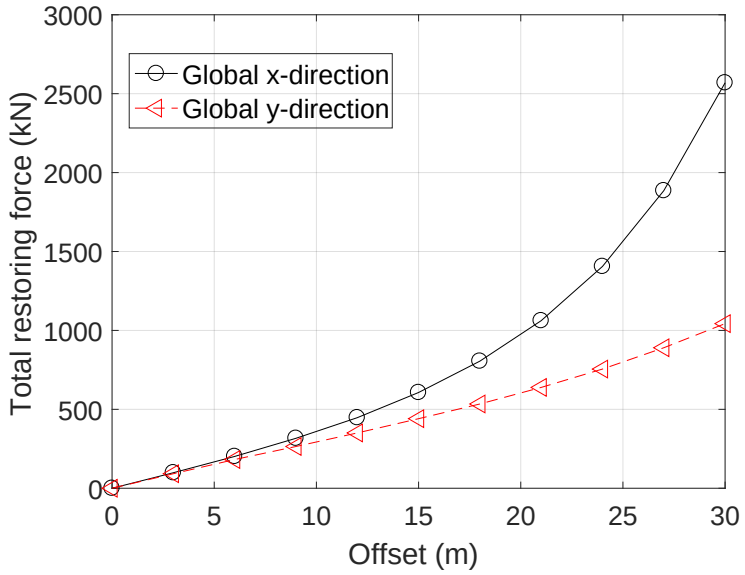

Figure 15: Restoring characteristics of the mooring system (the global coodinate system is earth-fixed and initially aligned with the body coordinate system of the spar).

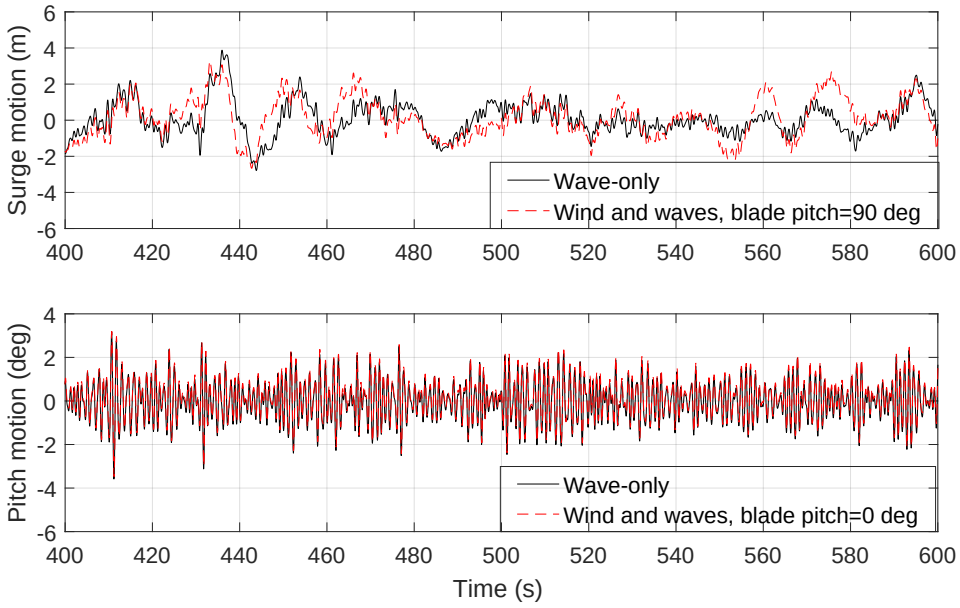

Figure 16: Time history of the catamaran motion responses, H_s=2.5 m, T_p=12 s, β=0 deg, Seed 1 (surge motion with the mean value removed).

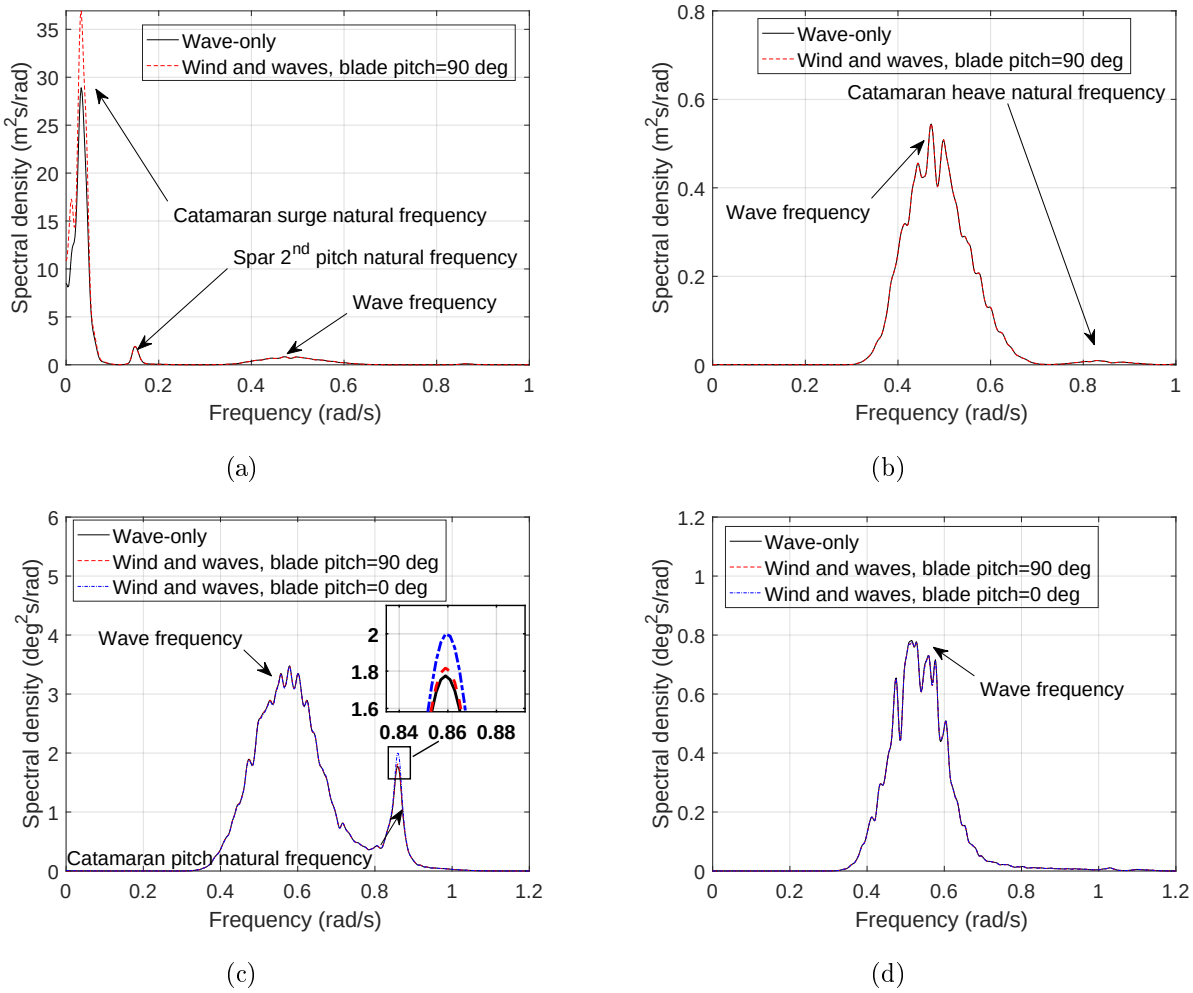

Figure 17: Motion response spectra of the catamaran, H_s=2.5 m, T_p=12 s: (a) surge motion, β=0 deg; (b) heave motion, β=0 deg; (c) pitch motion, β=0 deg; (d) roll motion, β=30 deg (the spectra are obtained using the WAFO toolbox [49]).

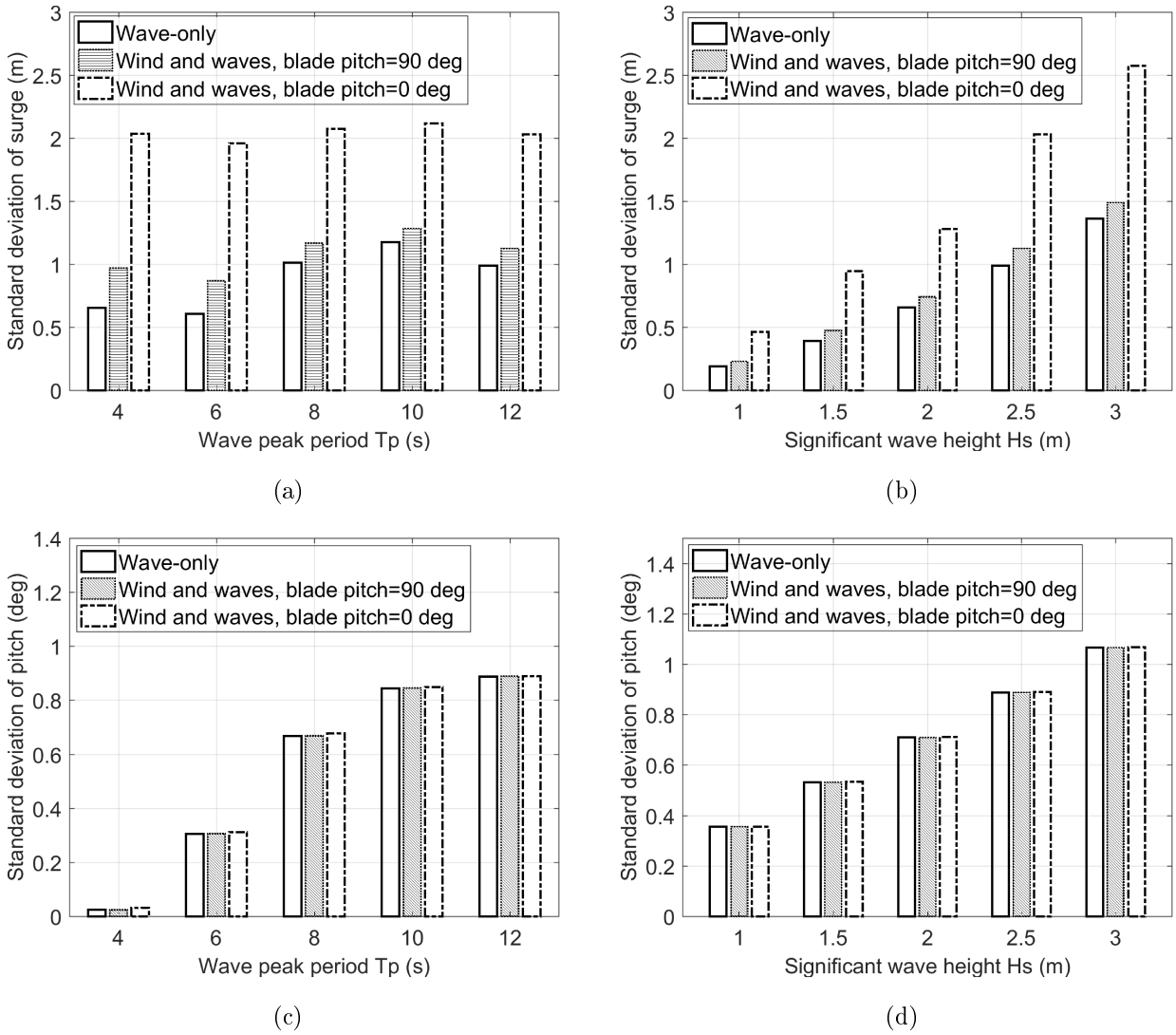

Figure 18: Standard deviations of the catamaran motion responses, β=0 deg: (a)H_s=2.5 m, surge motion; (b) T_p=12 s, surge motion; (c) H_s=2.5 m, pitch motion; (d) T_p=12 s, pitch motion.

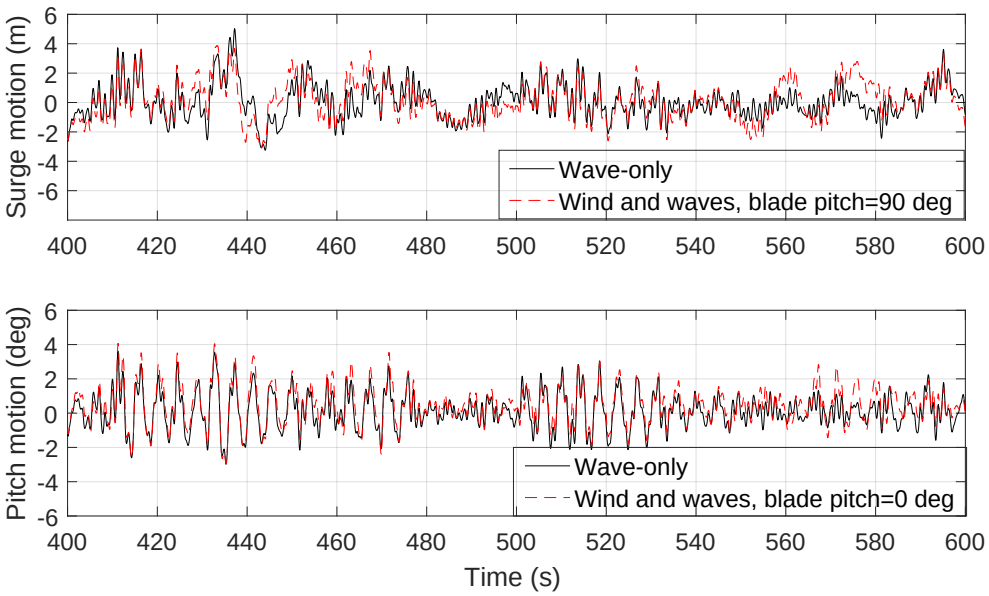

Figure 19: Time history of the spar motion responses, H_s=2.5 m, T_p=12 s, β=0 deg, Seed 1 (surge motion with the mean value removed).

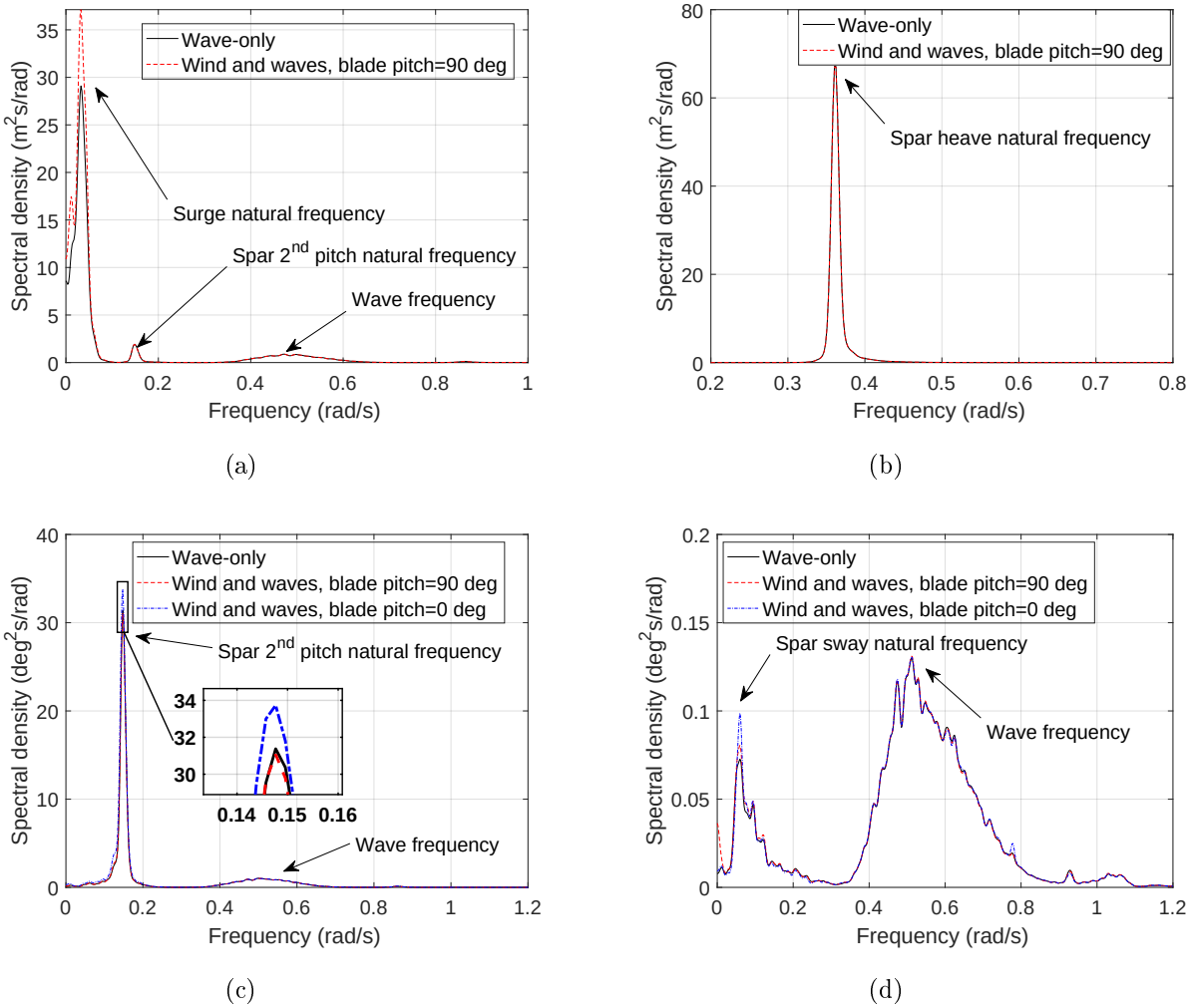

Figure 20: Comparison of the motion response spectra of the spar foundation, H_s=2.5 m, T_p=12 s: (a) surge motion, β=0 deg; (b) heave motion, β=0 deg; (c) pitch motion, β=0 deg; (d) roll motion, β=30 deg.

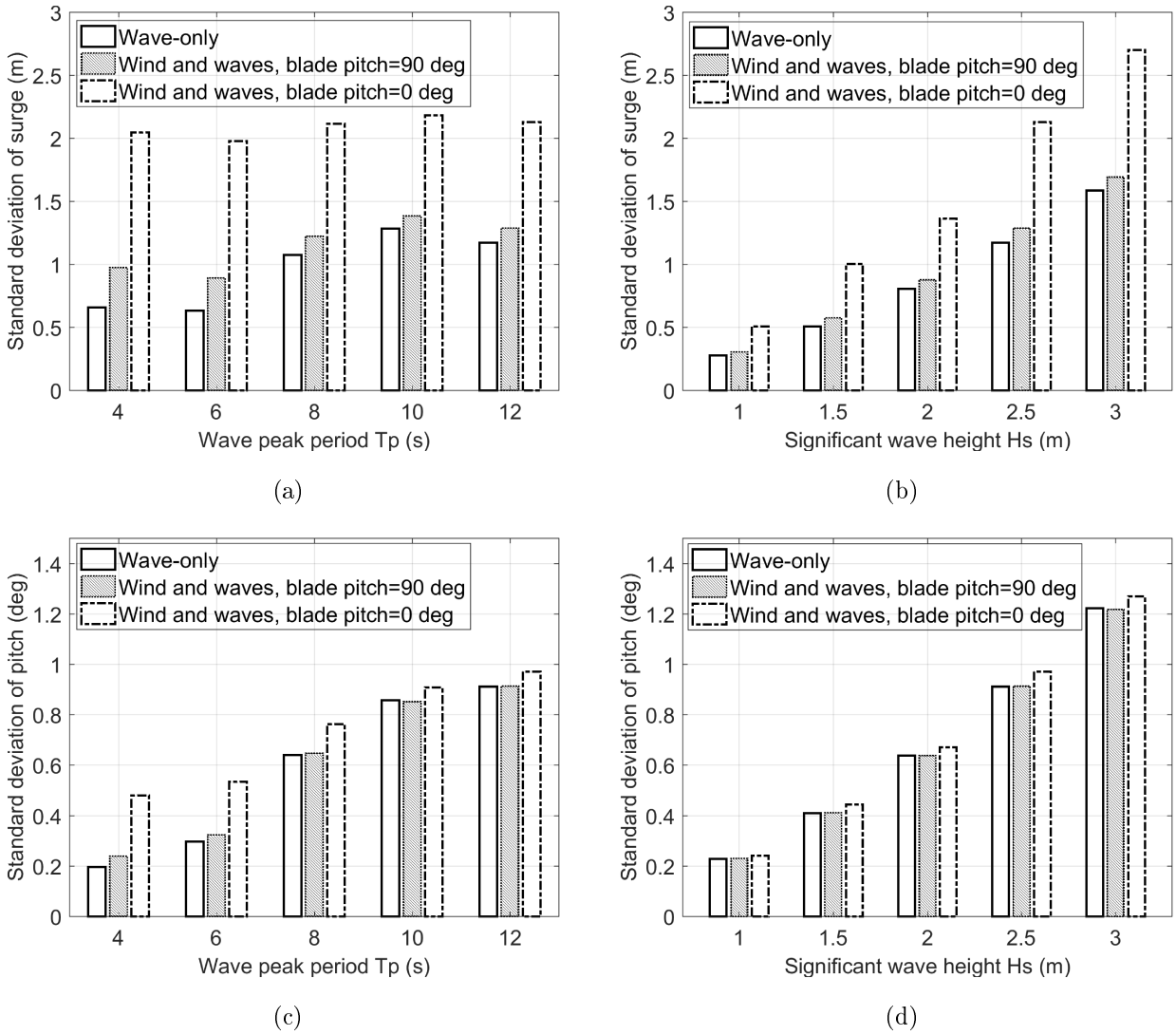

Figure 21: Standard deviations of the spar motion responses: (a) H_s=2.5 m, surge motion; (b) T_p=12 s, surge motion; (c) H_s=2.5 m, pitch motion; (d) T_p=12 s, pitch motion.

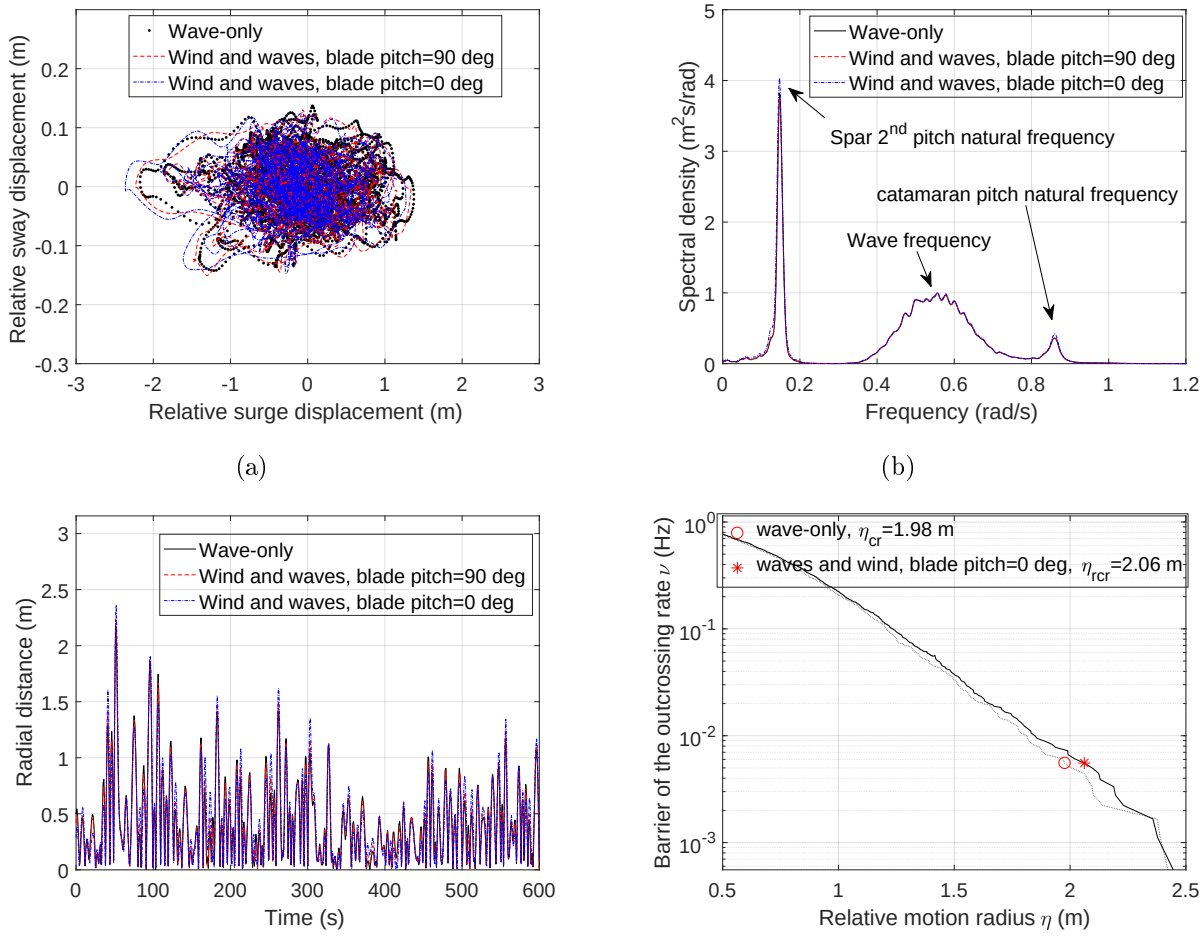

Figure 22: Relative motions between catamaran and spar at the mating point, H_s=2.5 m, T_p=12 s, β=0 deg, Seed 1: (a) position of the mating point in the horizontal plane; (b) response spectrum of the relative surge motion; (c) time history of the relative motion radius $\eta = \sqrt{x^2 + y^2}$; (d) variation of the outcrossing rate with relative motion radius, the marked points corresponding to ν_{cr}=$5.5 \cdot 10^{-3}$ Hz.

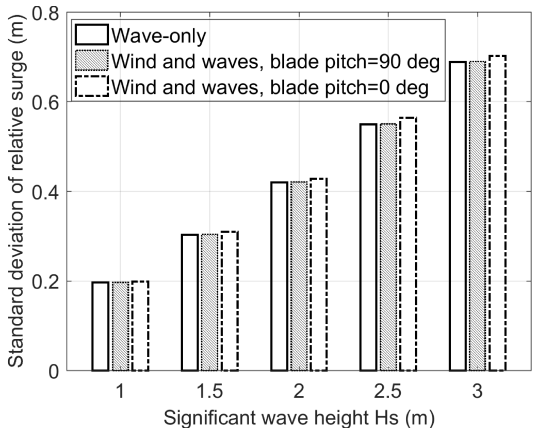

(a)

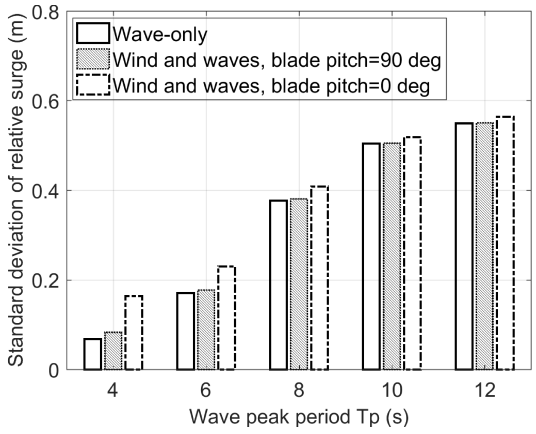

(b)

Figure 23: Standard deviations of the relative surge motion at the mating point, β=0 deg: (a) T_p=12 s; (b) H_s=2.5 m.

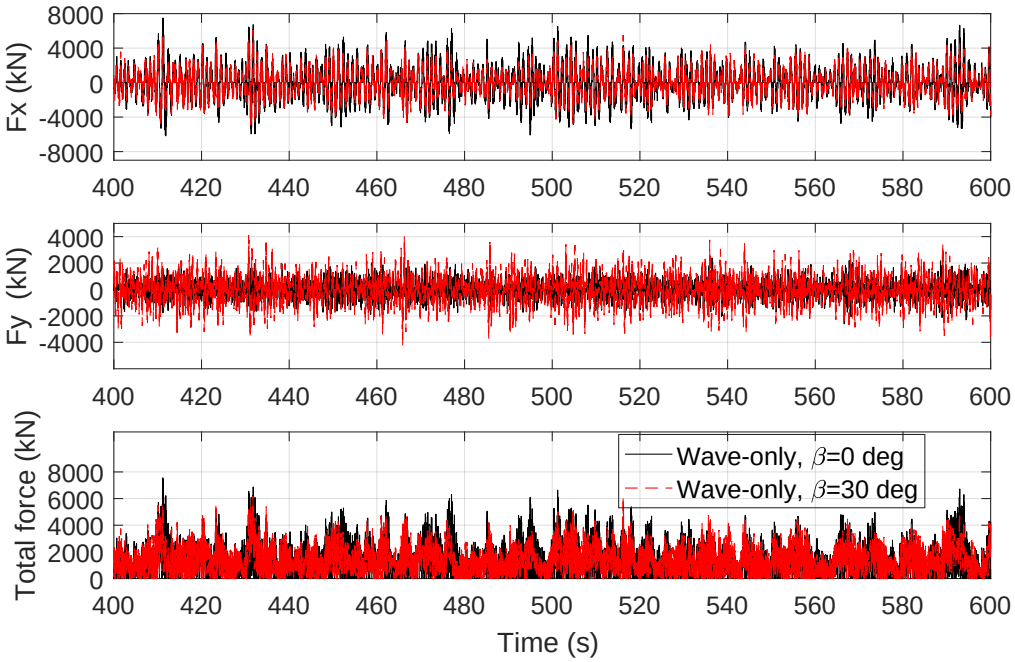

Figure 24: Time history of the forces on the sliding grippers, H_s=2.5 m, T_p=12 s, β=0 deg, Seed 1.

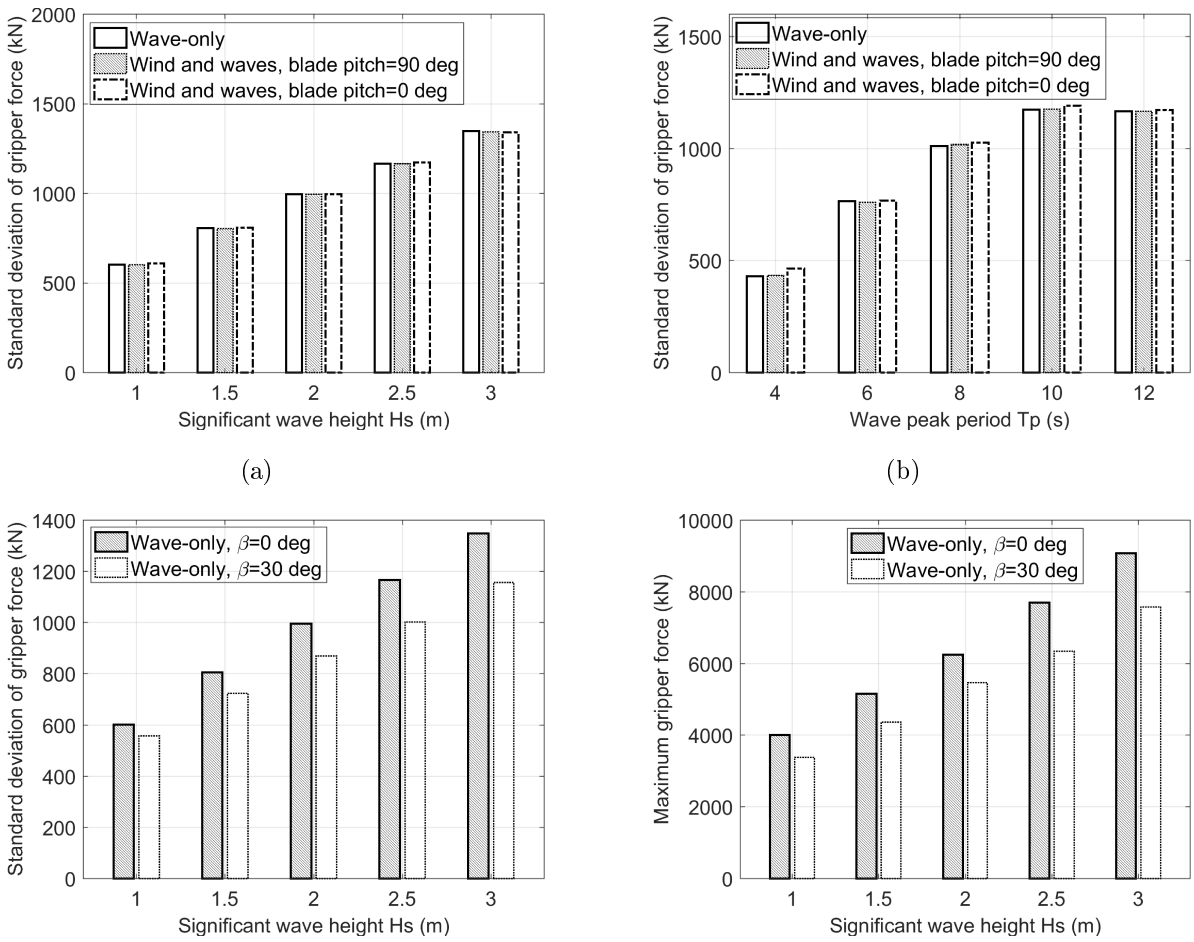

Figure 25: Statistics of the total forces on the sliding grippers: (a) standard deviation, T_p=12 s, β=0 deg; (b) standard deviation, H_s=2.5, β=0 deg; (c) standard deviation, T_p=12 s, wave-only; (d) maximum, T_p=12 s, wave-only.

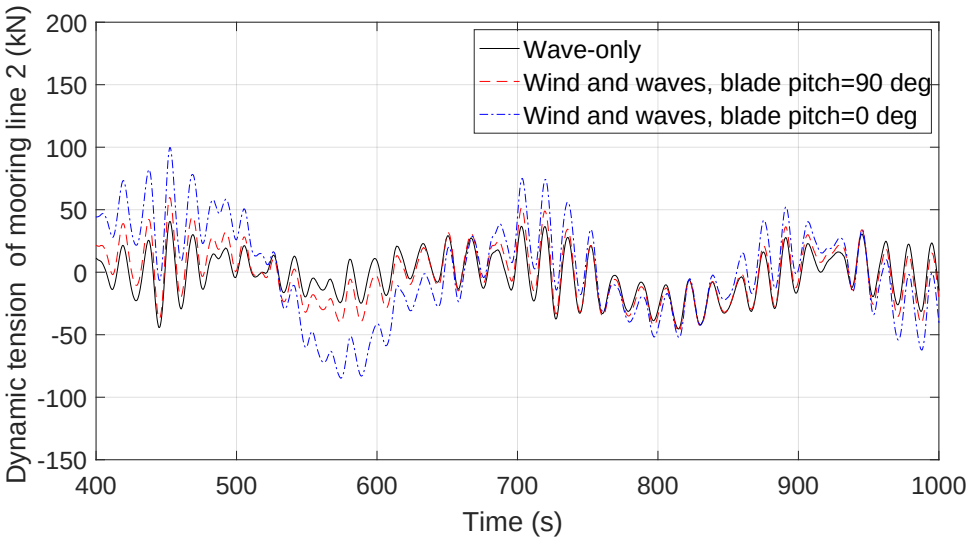

Figure 26: Time history of the dynamic tension in mooring line 2, H_s=2.5 m, T_p=12 s, β=0 deg, Seed 1 (mean tension close to 700 kN).

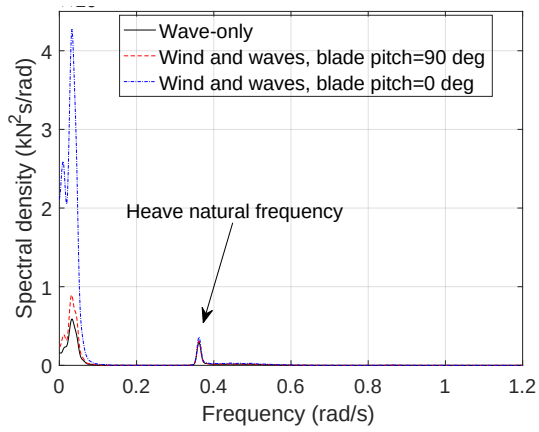

(a)

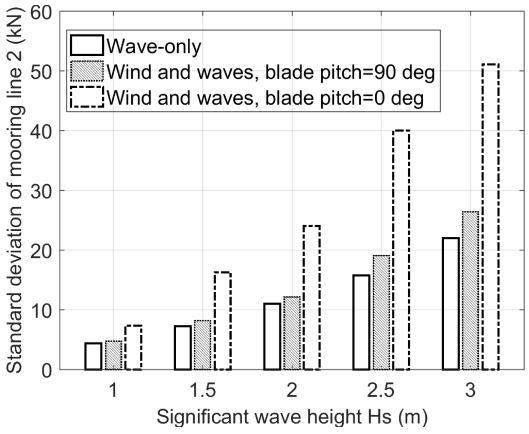

(b)

Figure 27: Spectra and statistics of mooring line 2 force: (a) response spectrum of mooring line tension, H_s=2.5 m, T_p=12 s, β=0 deg; (b) standard deviation, T_p=12 s, β=0 deg.